Humanoid robots - Physical human-robot interaction II

Doc. Mgr. Matěj Hoffmann, Ph.D.

Outline

- Human safety and injury - biomechanical criteria
- Impacts and their modeling
- Physical human robot collaboration - power and force limiting (PFL)
- Collision detection, isolation, identification, …, reaction
- Combining speed and separation monitoring and power and force limiting

ISO 10218-2 – Types of human-robot-collaboration

1. Safety-rated monitored stop
   - Robot in normal automatic mode
   - Robot stops when human enters the workspace and resumes automatically after leaving
2. Hand guided operation
   - Robot operates at low speed
   - Operation only with enabling switch
3. Speed and separation monitoring
   - Robot operates autonomously at low speed
   - Robot stops when distance to human gets too small
4. Power and force limiting
   - Restriction of force and power of the robot
   - Contact between human and robot allowed

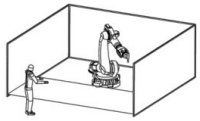

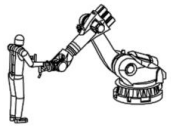

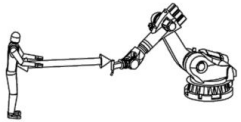

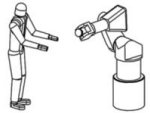

14

Fraunhofer IPA

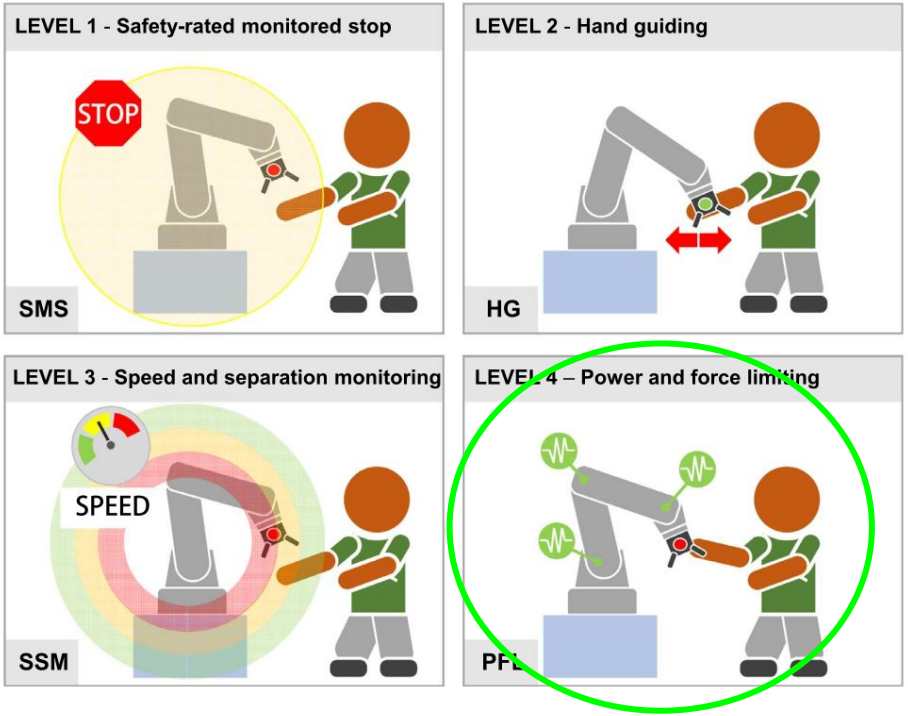

Slide from: Theo Jacobs, Fraunhofer IPA, Safety standards and risk assessment for robots, 2016

Villani, V., Pini, F., Leali, F., & Secchi, C. (2018). Survey on human–robot collaboration in industrial settings: Safety, intuitive interfaces and applications. *Mechatronics*, *55*, 248-266.

Contact scenarios

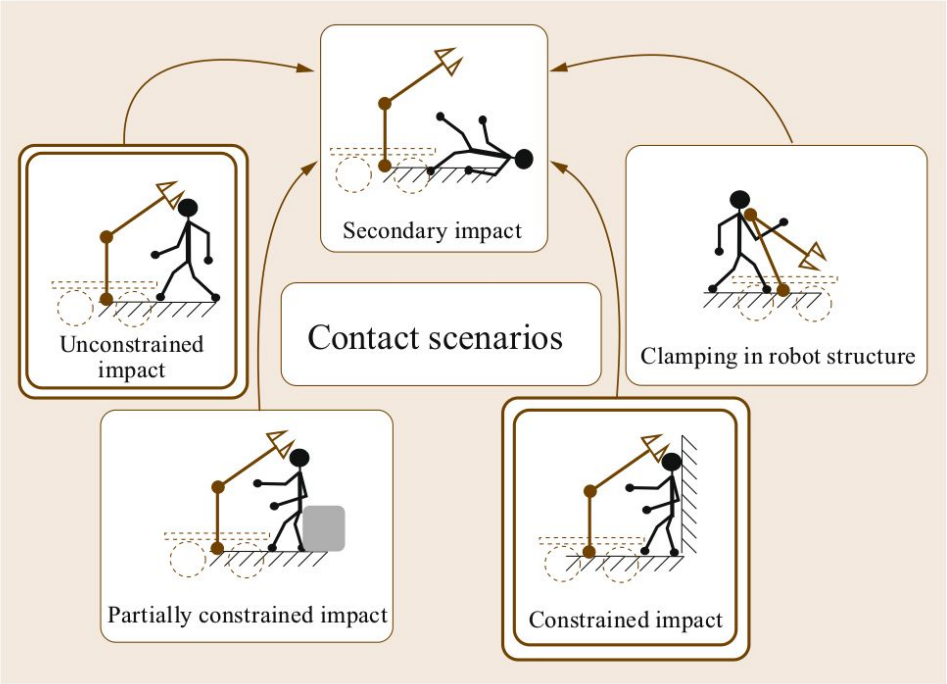

http://handbookofrobotics.org/view-chapter/69/videodetails/608

S. Haddadin, A. Albu-Schäffer, M. Strohmayr, M. Frommberger, G. Hirzinger: Injury evaluation of human-robot impacts, Proc. IEEE Int. Conf. Robot. Autom. (ICRA), Pasadena (2008), pp. 2203 – 2204; doi: 10.1109/ROBOT.2008.4543534.

Fig. 69.4 Robot–human impact scenario classes. Unconstrained and constrained impacts are considered the two main scenarios

Haddadin, S., & Croft, E. (2016). Physical human–robot interaction. In *Springer handbook of robotics* (pp. 1835-1874). Springer, Cham.

Power and force limiting

- types of contact events for robot systems specifically designed for power and force limiting
- robot-workpiece-human contacts can occur intentionally or not

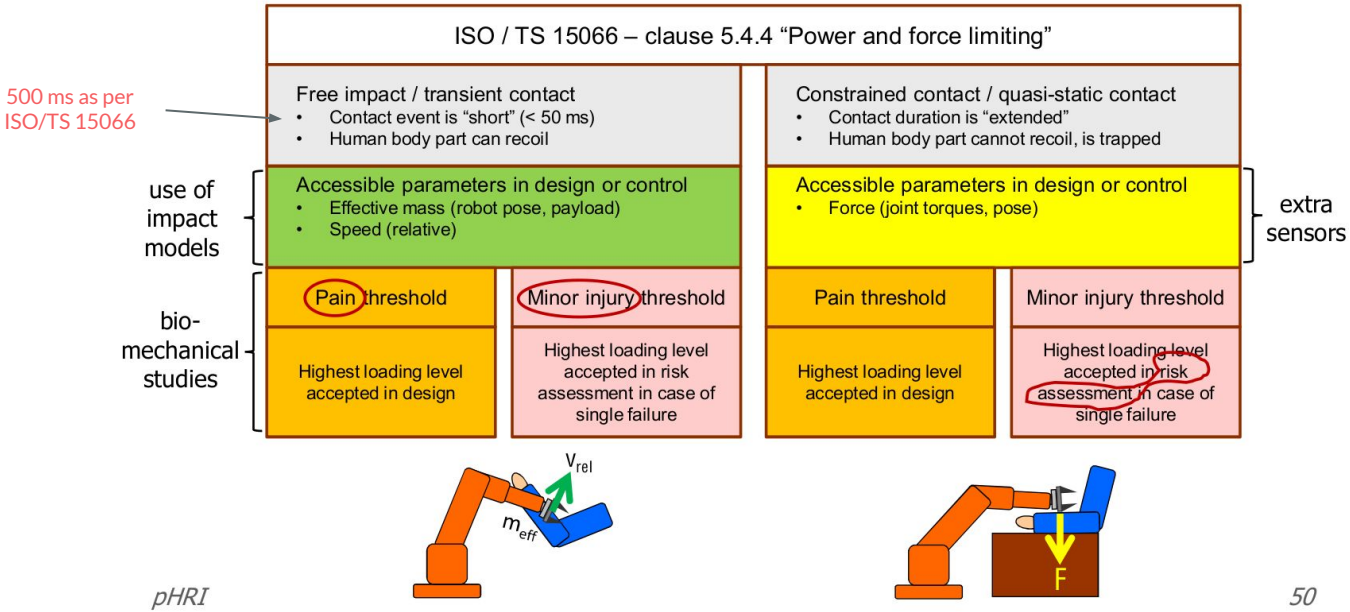

Slide from Alessandro de Luca: Physical HRI. http://www.diag.uniroma1.it/deluca/pHRI_elective/pHRI_SafetyDependability.pdf

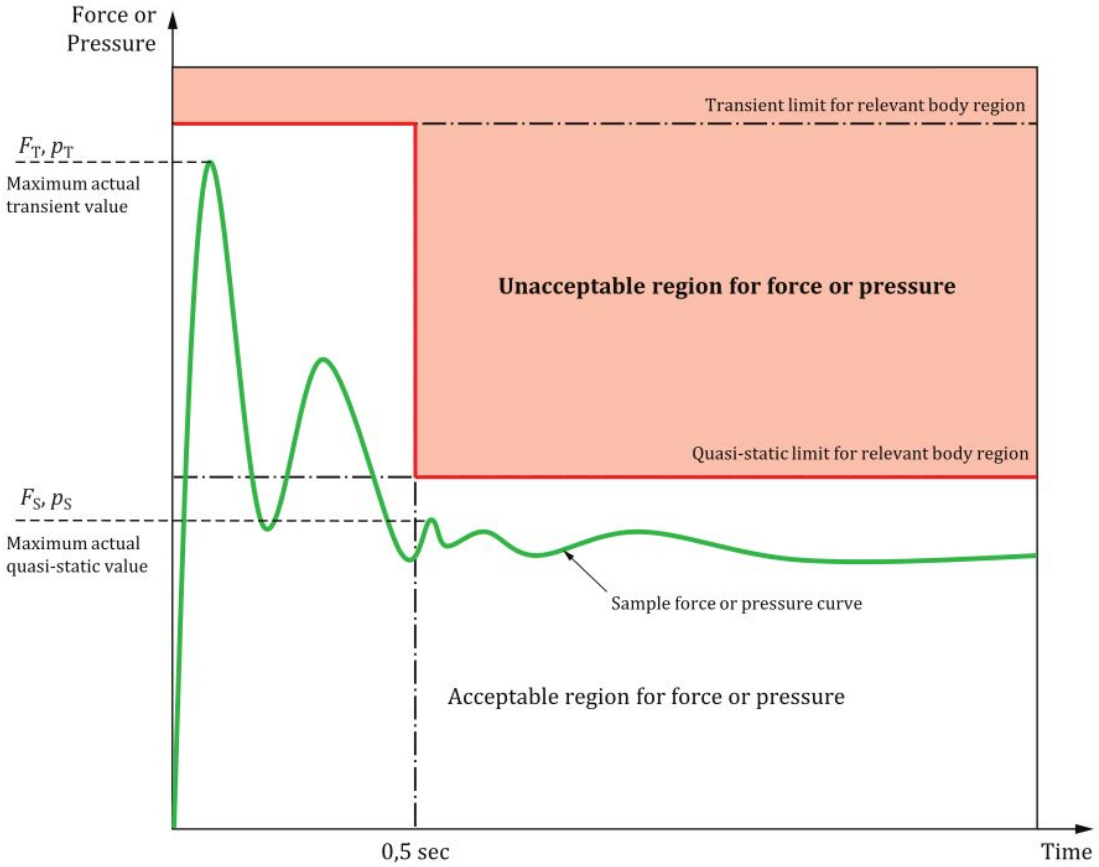

Figure 4 — Graphical representation of acceptable and unacceptable forces or pressures

ISO/TS 15066:2016
Robots and robotic devices — Collaborative robots

Biomechanical criteria in TS 15066

$80\ W/150\ N$ power and force limits were present in ISO 10218-1:2006 but have been removed in 2011!

"onset of pain" studies

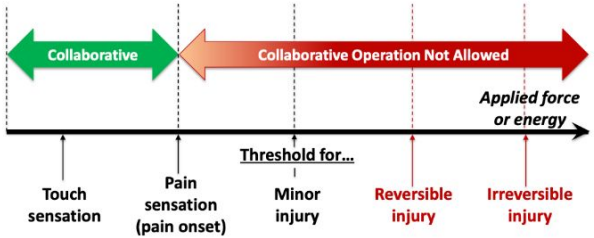

$$1\ W = 1\ N\frac{m}{s} = 1\frac{kg\ m^2}{s^3}$$

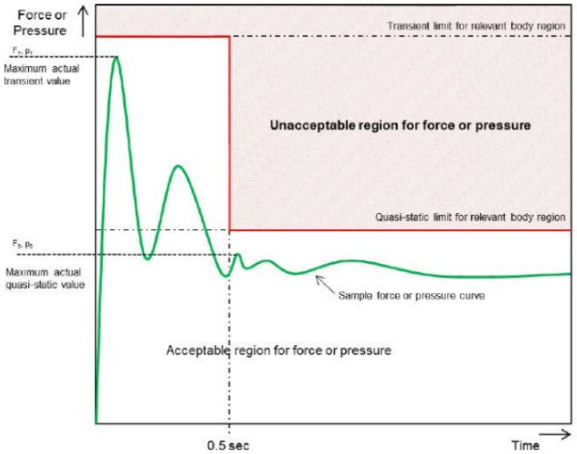

- force applied where (body part)?
- clamping conditions?

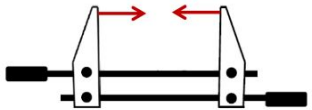

Slide from Alessandro de Luca: Physical HRI. http://www.diag.uniroma1.it/deluca/pHRI_elective/pHRI_SafetyDependability.pdf

Biomechanical criteria in TS 15066

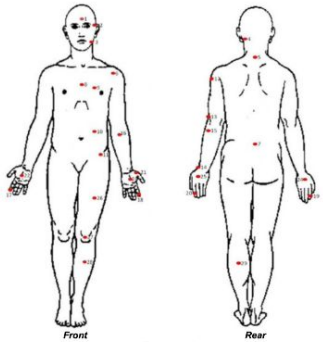

Body Region		Specific Body Area	Quasi-Static Contact: Maximum Allowable Pressure p_s [N/cm2] (see NOTE 1)	Quasi-Static Contact: Maximum Allowable Force [N] (see NOTE 2)	Transient Contact: Maximum Allowable Pressure Multiplier P_T (see NOTE 3)	Transient Contact: Maximum Allowable Force Multiplier F_T (see NOTE 3)
Skull and forehead	1	Middle of forehead	125	130	N/A	N/A
	2	Temple	110		N/A	
Face	3	Masticatory muscle	110	65	N/A	N/A
Neck	4	Neck muscle	138	145	2	2
	5	Seventh neck muscle	205		2	
Back and shoulders	6	Shoulder joint	155	210	2	2
	7	Fifth lumbar vertebra	213		2	2
Chest	8	Sternum	116	140	2	2
	9	Pectoral muscle	166		2	
Abdomen	10	Abdominal muscle	143	110	2	2
Pelvis	11	Pelvic bone	209	180	2	2
Upper arms and elbow joints	12	Deltoid muscle	192	150	2	2
	13	Humerus	216		2	
Lower arms and wrist joints	14	Radial bone	192	160	2	2
	15	Forearm muscle	181		2	
	16	Arm nerve	179		2	
Hands and fingers	17	Forefinger pad D	298	135	2	2
	18	Forefinger pad ND	273		2	
	19	Forefinger end joint D	275		2	
	20	Forefinger end joint ND	219		2	
	21	Thenar eminence	203		2	
	22	Palm D	256		2	
	23	Palm ND	260		2	
	24	Back of the hand D	197		2	
	25	Back of the hand ND	193		2	
Thighs and knees	26	Thigh muscle	246	220	2	2
	27	Kneecap	223		2	
Lower legs	28	Middle of shin	220	125	2	2
	29	Calf muscle	212		2	

CRITICAL ZONE

from studies by the University of Mainz

Slide from Alessandro de Luca: Physical HRI. http://www.diag.uniroma1.it/deluca/pHRI_elective/pHRI_SafetyDependability.pdf

Biomechanical criteria in TS 15066

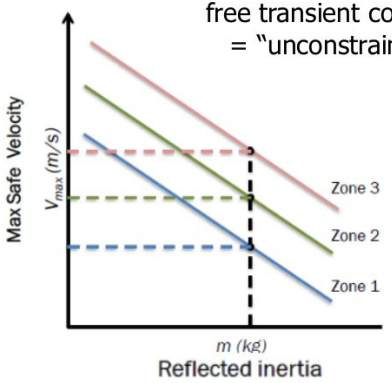

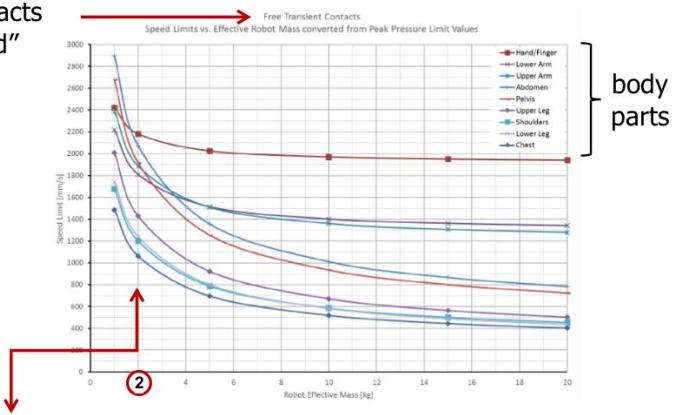

... from the Handbook of Injury in SAPHARI

Body region	Speed limit [mm/sec] as a function of robot effective mass (m_R) based on maximum pressure value (p_{max}) with an area (A) of 1 cm²					
	1	2	5	10	15	20
Hand/finger	2 400	2 200	2 000	2 000	2 000	1 900
Lower arm	2 200	1 800	1 500	1 400	1 400	1 300
Upper arm	2 400	1 900	1 500	1 400	1 300	1 300
Abdomen	2 900	2 100	1 400	1 000	870	780
Pelvis	2 700	1 900	1 300	940	800	720
Upper leg	2 100	1 500	1 000	810	730	680
Lower leg	1 900	1 400	1 000	900	840	810
Shoulders	1 700	1 200	790	590	500	450
Chest	1 500	1 100	700	520	440	400

Slide from Alessandro de Luca: Physical HRI. http://www.diag.uniroma1.it/deluca/pHRI_elective/pHRI_SafetyDependability.pdf

Impacts and their modeling

Transient contact model according to ISO/TS 15066.

Fully inelastic collision.

- Kinetic energy is not conserved, and will change forms into sound, heat, radiation, or some other form.
- Good news or bad news?
- Assumption here: Energy fully deposited in affected body region.
- Worst case assumption.

Contact area A = 1 cm^2.

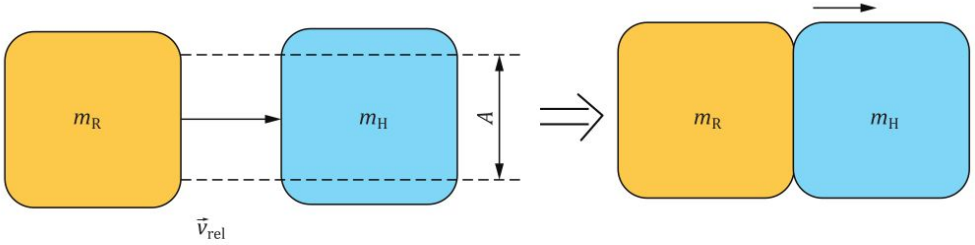

Key

A	area of contact between robot and body region
m_H	effective mass of human body region
m_R	effective mass of robot as a function of robot posture and motion
v_{rel}	relative speed between robot and human body region

Figure A.2 — Contact model for transient contact

Impactor shapes

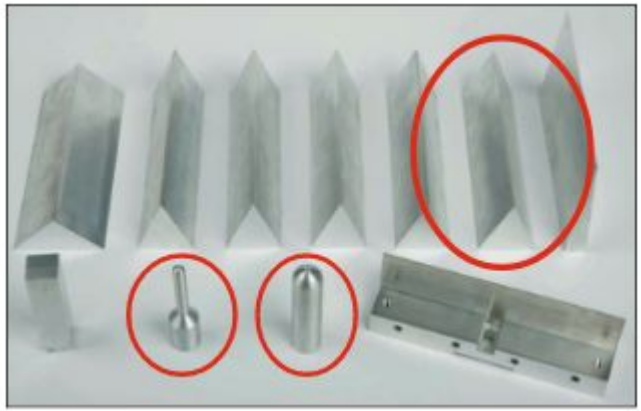

Haddadin, S., Haddadin, S., Khoury, A., Rokahr, T., Parusel, S., Burgkart, R., ... & Albu-Schäffer, A. (2012). On making robots understand safety: Embedding injury knowledge into control. *The International Journal of Robotics Research*, *31*(13), 1578-1602.

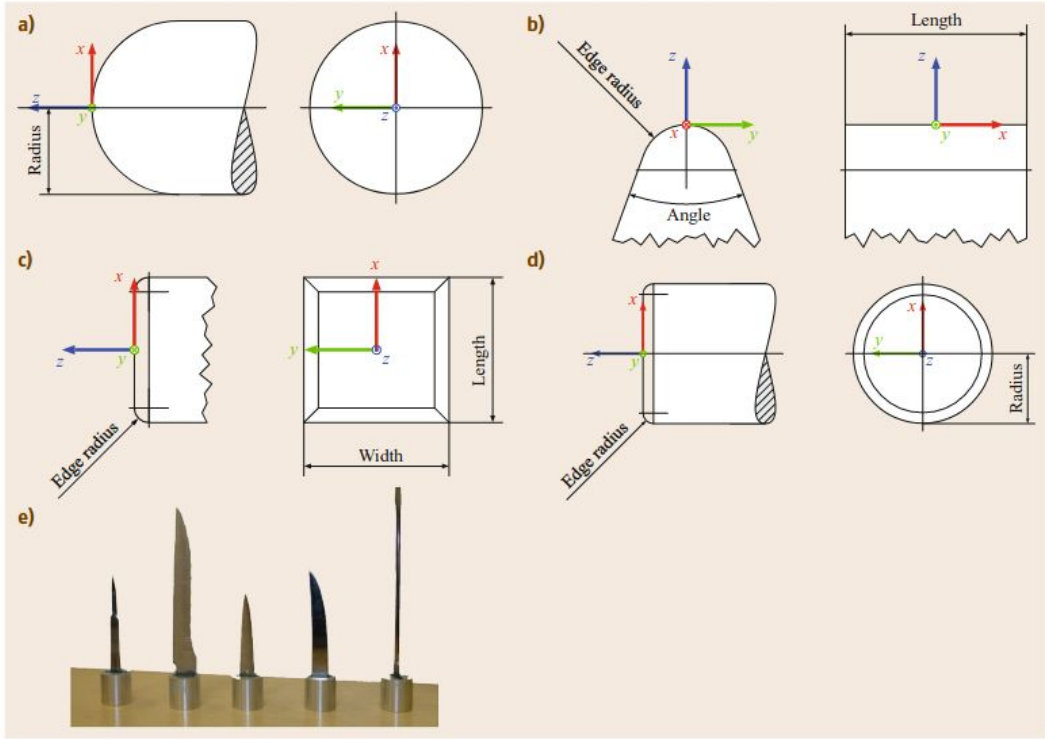

Fig.69.5a–e Typical impactor primitives with according parameters. **(a)** Sphere, **(b)** edge, **(c)** cuboid, **(d)** flat circular, **(e)** sharp tools

Haddadin, S., & Croft, E. (2016). Physical human–robot interaction. In *Springer Handbook of Robotics* (pp. 1835-1874). Springer, Cham.

Impactor evaluation

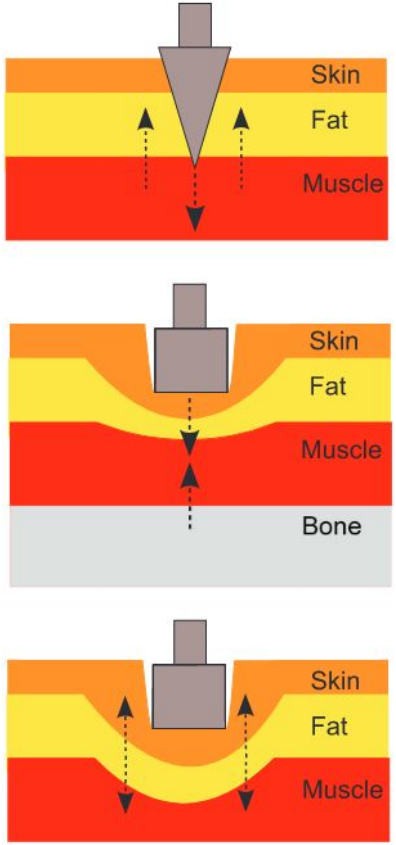

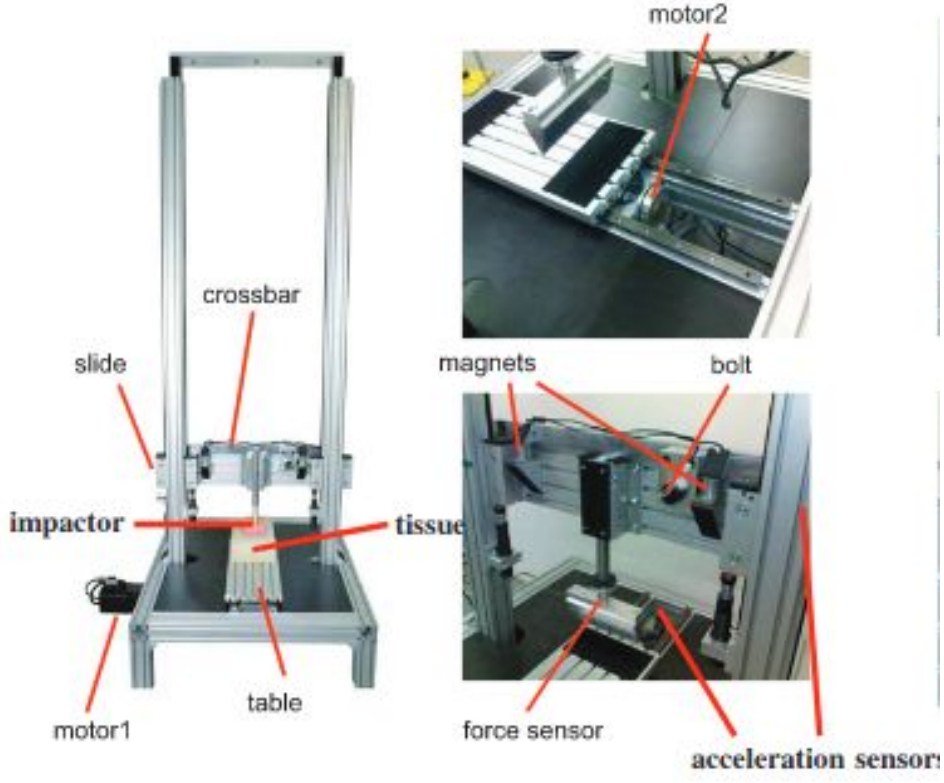

Haddadin, S., Haddadin, S., Khoury, A., Rokahr, T., Parusel, S., Burgkart, R., ... & Albu-Schäffer, A. (2012). On making robots understand safety: Embedding injury knowledge into control. *The International Journal of Robotics Research*, *31*(13), 1578-1602.

Influence of Robot Mass and Velocity. Assume a simple mass–spring-mass model for the impact between human and robot. M_H is the reflected inertia of the human. K_H is the contact stiffness, which is in the case of a rigid robot mainly the effective stiffness of the human contact area. $\dot{x}_{re}^0$ is the relative impact velocity between the robot and human. Solving the corresponding differential equation leads to the maximum contact force

$$\mathcal{F}_{ext}^{max} = \sqrt{\frac{m_u M_H}{m_u + M_H}} \sqrt{K_H} \dot{x}_{re}^0 .$$

m_u ... effective mass of a robot acting in the instantaneous collision direction

Haddadin, S., & Croft, E. (2016). Physical human–robot interaction. In *Springer Handbook of Robotics* (pp. 1835-1874). Springer, Cham.

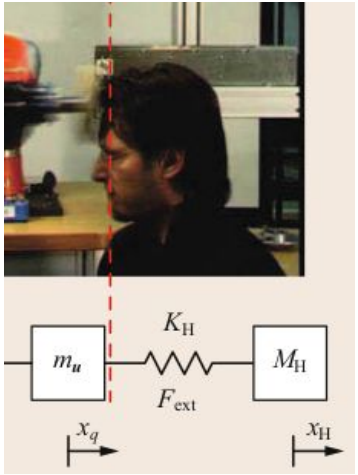

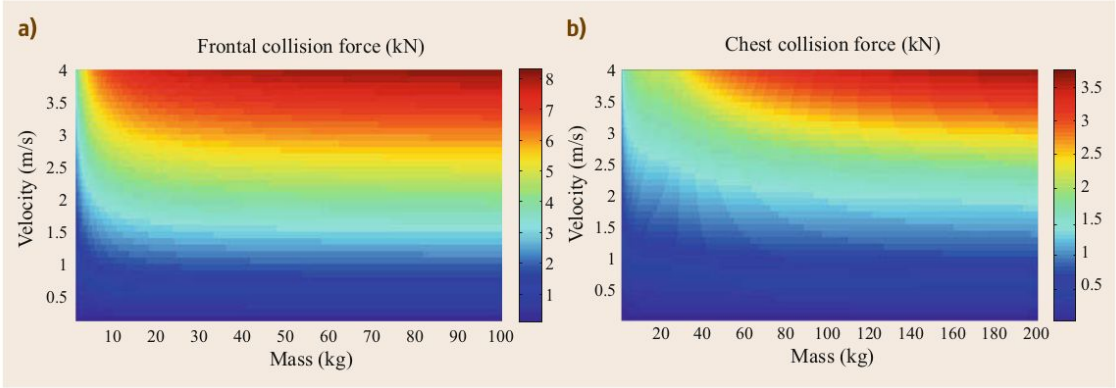

Fig.69.7a,b Mass–velocity dependency for (a) human head and (b) chest contact force. A mass–spring-mass model is used for collisions against the head, where the head mass M_H is 4.5 kg and the approximate contact stiffness of the frontal bone $K_H = 1000\,N/mm$ (after [69.33]). For the chest, the model proposed in [69.47] is used

Influence of robot mass and velocity

Assume a simplifying decoupling of the head from the torso, which holds for the short duration of the impact. For the post-impact phase, neck stiffness and body inertia have to be considered, which complicates the analysis considerably. The dependency of frontal bone contact force on the robot mass and velocity is depicted in Fig. 69.7a. It can be observed that collision force (which is a well-known bone fracture indicator) generally increases with velocity. For increasing mass, however, a saturation effect takes place. After a certain robot mass has been reached ($m_u \approx 20\,\mathrm{kg}$ in Fig. 69.7), additional weight has only negligible influence on collision force. This inertial saturation effect can also be observed for other impact locations, such as contacts with the chest (Fig. 69.7b).

If the robot mass is significantly larger than the human head mass, that is, $m_u \gg M_\mathrm{H}$, (69.8) reduces to

$$\mathcal{F}_\mathrm{ext}^\mathrm{max}(m_u \gg M_\mathrm{H}) = \sqrt{K_\mathrm{H} M_\mathrm{H}}\,\dot{x}_\mathrm{re}^0 \,. \qquad (69.9)$$

This shows that for a robot with significantly larger reflected inertia than the human head, only the contact stiffness, the impact velocity, and the mass of the human head are relevant but not the robot mass.

The $m_u >> M_H$ assumption is often used for contacts with the human hand.

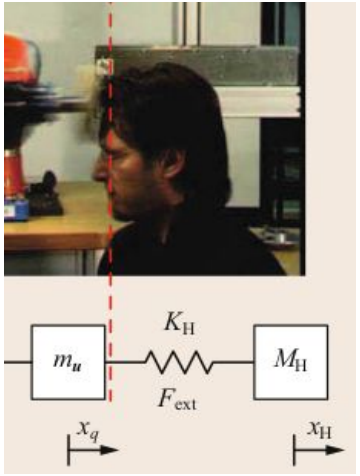

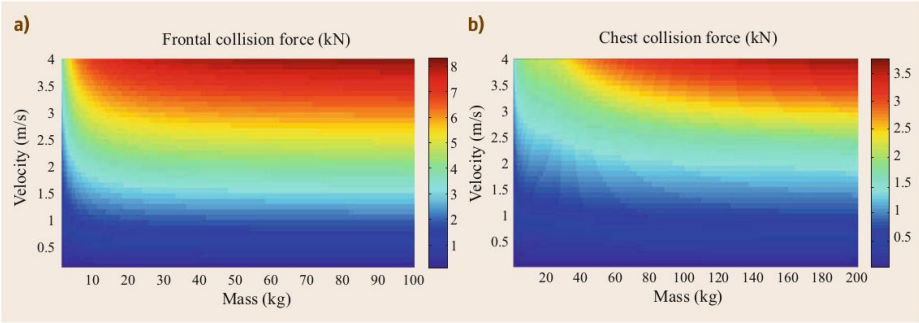

Fig.69.7a,b Mass–velocity dependency for **(a)** human head and **(b)** chest contact force. A mass–spring-mass model is used for collisions against the head, where the head mass M_H is 4.5 kg and the approximate contact stiffness of the frontal bone $K_\mathrm{H} = 1000\,\mathrm{N/mm}$ (after [69.33]). For the chest, the model proposed in [69.47] is used

Haddadin, S., & Croft, E. (2016). Physical human–robot interaction. In *Springer Handbook of Robotics* (pp. 1835-1874). Springer, Cham.

Modification of power and force limits

an example of risk critical task …
mitigated by application re-design

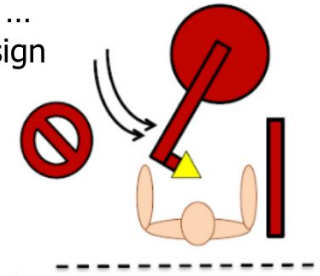

1. Eliminate pinch and crush points
2. Reduce robot system inertia or mass
3. Reduce robot system velocity

   2. & 3. will reduce energy transfer in a collision
4. Modify robot posture such that contact surface area is increased
5. Avoid sensitive body areas (head & neck)

\+ Safe control: collision detection & reaction

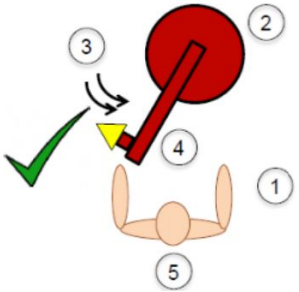

Slide from Alessandro de Luca: Physical HRI. http://www.diag.uniroma1.it/deluca/pHRI_elective/pHRI_SafetyDependability.pdf

Factors affecting safety in the PFL regime

- Robot velocity
  - constraints: cycle time of the application
- Robot mass
  - physical mass and its distribution
  - effective mass
- Impactors
  - shape - blunt or sharp
  - stiffness
- Collision reaction

Safe design

- Lightweight
  - high-strength metals, or composite materials for the robot links
- Tendon-based robots
  - Remote direct drives - actuators in robot base.
  - Low reduction ratios -> back-driveability.
- Elastic actuation
  - Series Elastic Actuation (SEA)
  - Variable Stiffness Actuation (VSA)
  - Variable Impedance Actuations (VIA) - stiffness & damping

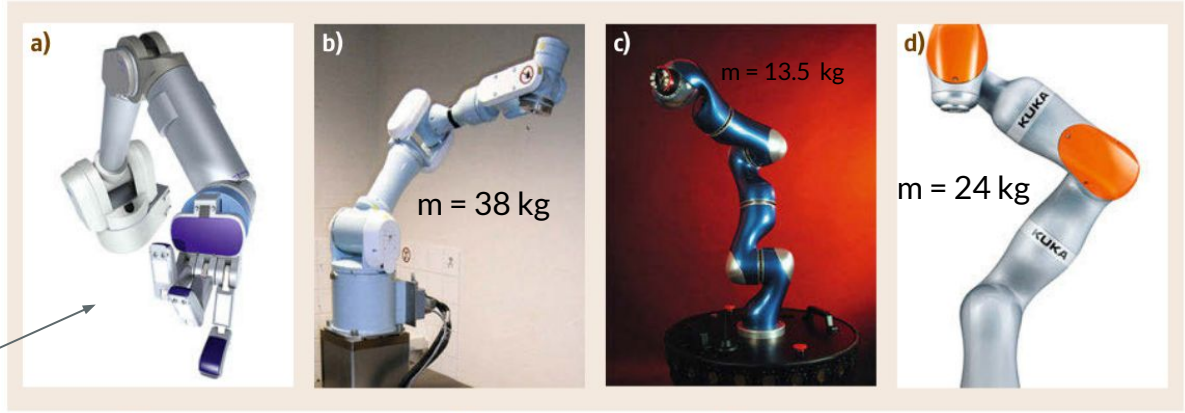

Fig. 69.10 (a) Barrett arm (after [69.58]), (b) Mitsubishi PA10 arm, (c) DLR lightweight robot III (after [69.59]), (d) KUKA LBR iiwa (after [69.60]) (courtesy of Barret Technology Inc., DLR, KUKA)

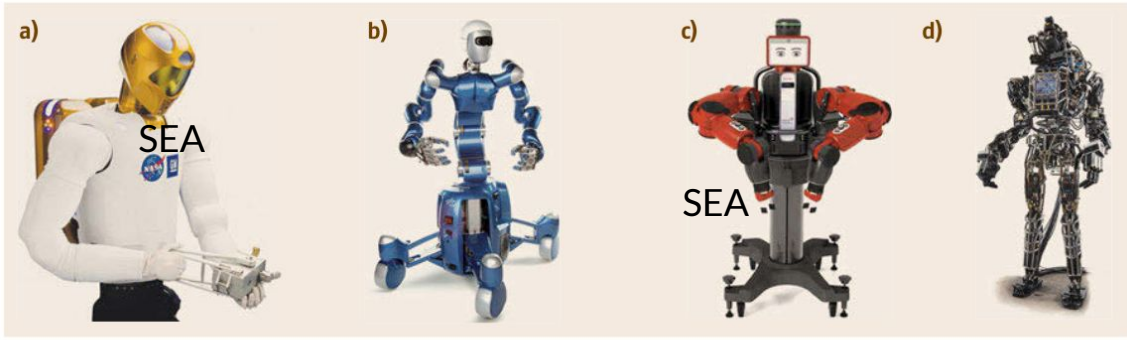

Fig. 69.11 (a) NASA *Robonaut 2*, (b) DLR *Rollin' Justin*, (c) Rethink Robotics *Baxter* and (d) Boston Dynamics *Atlas* (courtesy of NASA, DLR, Rethink Robotics Inc., Boston Dynamics)

Haddadin, S., & Croft, E. (2016). Physical human–robot interaction. In *Springer handbook of robotics* (pp. 1835-1874). Springer, Cham.

Robot dynamics - joint space

To model impact forces, robot dynamics has to be considered.

Equation of motion: $F = ma$

Robot equation of motion: $\boldsymbol{\tau} = \boldsymbol{M}(\boldsymbol{q})\ddot{\boldsymbol{q}} + \boldsymbol{C}(\boldsymbol{q}, \dot{\boldsymbol{q}})\dot{\boldsymbol{q}} + \boldsymbol{g}(\boldsymbol{q})$

$\boldsymbol{M}(\boldsymbol{q}) \in \mathbb{R}^{n \times n}$ is the symmetric and positive definite joint space inertia matrix.

- Function of the robot configuration.

Mass matrix examples

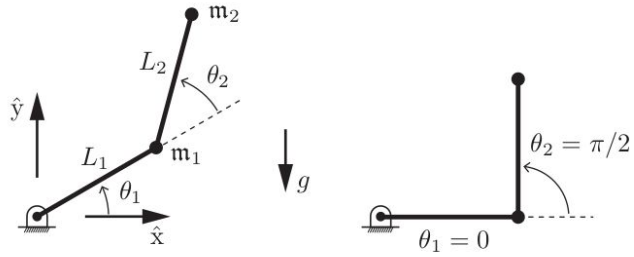

Figure 8.1: (Left) A 2R open chain under gravity. (Right) At $\theta = (0, \pi/2)$.

$$L_1 = L_2 = m_1 = m_2 = 1$$

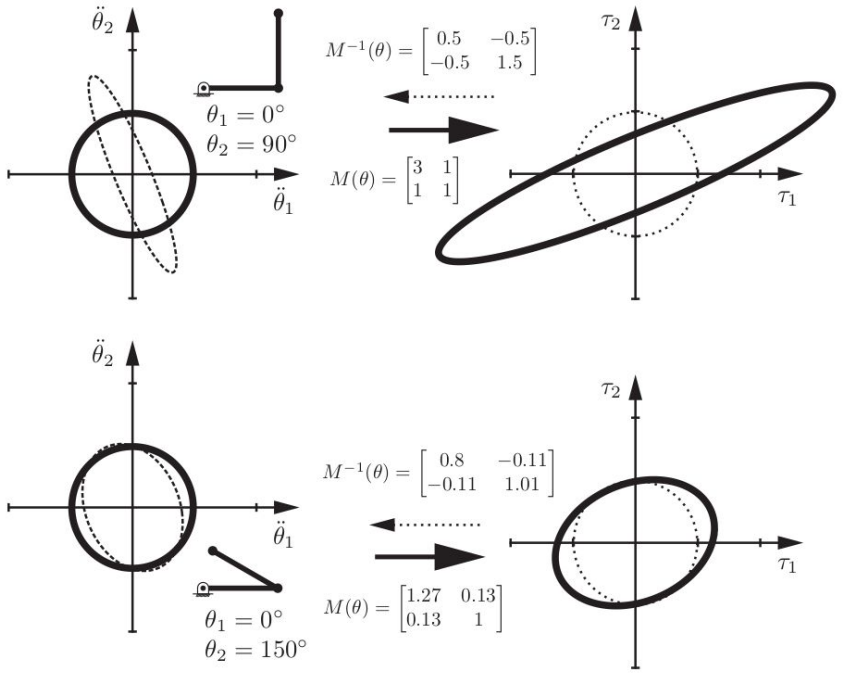

Figure 8.3: (Bold lines) A unit ball of accelerations in $\ddot{\theta}$ maps through the mass matrix $M(\theta)$ to a torque ellipsoid that depends on the configuration of the 2R arm. These torque ellipsoids may be interpreted as mass ellipsoids. The mapping is shown for two arm configurations: $(0°, 90°)$ and $(0°, 150°)$. (Dotted lines) A unit ball in τ maps through $M^{-1}(\theta)$ to an acceleration ellipsoid.

8.1.3 "Understanding the mass matrix" in Lynch, K. M., & Park, F. C. (2017). Modern robotics. Cambridge University Press.

https://modernrobotics.northwestern.edu/nu-gm-book-resource/8-1-3-understanding-the-mass-matrix

Robot dynamics – operational space

For assessing impacts, we need also operational space (end effector, or, more precisely, contact point) dynamics.

Mass matrix as effective mass at the end effector: $\Lambda(\theta)$

Robot kinetic energy must be the same regardless of coordinates (joint space or Cartesian space).
Kinetic energy for point masses ($\frac{1}{2}mv^2$) generalized:

$$\frac{1}{2}\dot{\theta}^{\mathrm{T}} M(\theta)\dot{\theta} = \frac{1}{2}V^{\mathrm{T}}\Lambda(\theta)V. \qquad (8.20)$$

Assuming the Jacobian $J(\theta)$ satisfying $V = J(\theta)\dot{\theta}$ is invertible, Equation (8.20) can be rewritten as follows:

$$\begin{aligned} V^{\mathrm{T}}\Lambda V &= (J^{-1}V)^{\mathrm{T}} M (J^{-1}V) \\ &= V^{\mathrm{T}}(J^{-T} M J^{-1})V. \end{aligned}$$

In other words, the end-effector mass matrix is

$$\Lambda(\theta) = J^{-T}(\theta)M(\theta)J^{-1}(\theta). \qquad (8.21)$$

8.1.3 “Understanding the mass matrix” in Lynch, K. M., & Park, F. C. (2017). Modern robotics. Cambridge University Press.

Originally developed in: Khatib, O. (1995). Inertial properties in robotic manipulation: An object-level framework. *The International Journal of Robotics Research*, *14*(1), 19-36.

Mass at the end effector

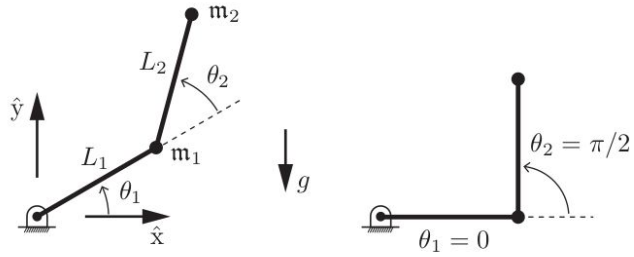

Figure 8.1: (Left) A 2R open chain under gravity. (Right) At $\theta = (0, \pi/2)$.

$$L_1 = L_2 = m_1 = m_2 = 1$$

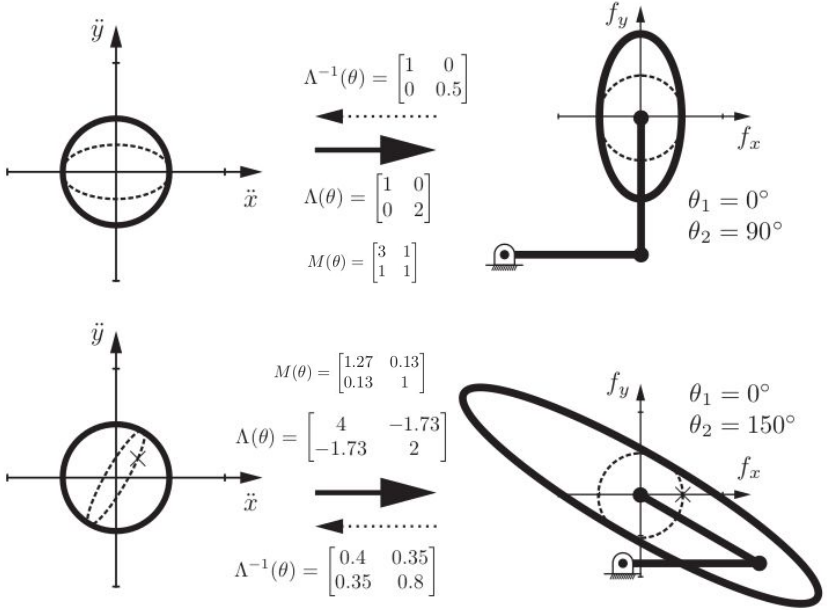

Figure 8.4: (Bold lines) A unit ball of accelerations in $(\ddot{x}, \ddot{y})$ maps through the end-effector mass matrix $\Lambda(\theta)$ to an end-effector force ellipsoid that depends on the configuration of the 2R arm. For the configuration $(\theta_1, \theta_2) = (0°, 90°)$, a force in the f_y-direction exactly feels both masses $\mathfrak{m}_1$ and $\mathfrak{m}_2$, while a force in the f_x-direction feels only $\mathfrak{m}_2$. (Dotted lines) A unit ball in f maps through $\Lambda^{-1}(\theta)$ to an acceleration ellipsoid. The $\times$ symbols for $(\theta_1, \theta_2) = (0°, 150°)$ indicate an example endpoint force $(f_x, f_y) = (1, 0)$ and its corresponding acceleration $(\ddot{x}, \ddot{y}) = (0.4, 0.35)$, showing that the force and acceleration at the endpoint are not aligned.

8.1.3 “Understanding the mass matrix” in Lynch, K. M., & Park, F. C. (2017). Modern robotics. Cambridge University Press.

https://modernrobotics.northwestern.edu/nu-gm-book-resource/8-1-3-understanding-the-mass-matrix

Effective mass in a certain impact direction

- Disregarding angular components at collision point.
  - Note: previous slide showing only $\Lambda_v(\theta)$

$v_{C_i} = J_{v_i}\dot{q}$

$\omega_i = J_{\omega_i}\dot{q}$

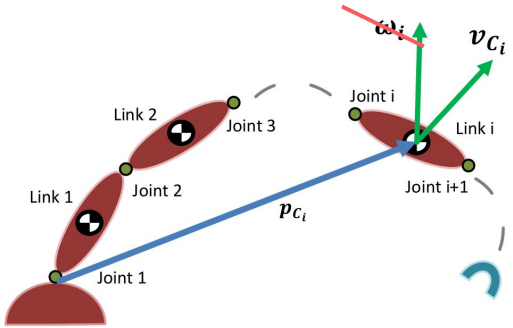

John Nassour, TU Chemnitz:
https://www.tu-chemnitz.de/informatik/KI/edu/robotik/ws2017/Dyn.pdf

- Imposing a certain collision direction $\boldsymbol{u}$.

$$\boldsymbol{\Lambda}(\boldsymbol{q}) = \left[\mathbf{J}_{\mathrm{c}}(\boldsymbol{q})\mathbf{M}(\boldsymbol{q})^{-1}\mathbf{J}_{\mathrm{c}}(\boldsymbol{q})^{\mathrm{T}}\right]^{-1}, \tag{69.5}$$

where the inverse of $\boldsymbol{\Lambda}(\boldsymbol{q})$ is based on the decomposition of the kinetic energy matrix

$$\boldsymbol{\Lambda}(\boldsymbol{q})^{-1} = \begin{bmatrix} \boldsymbol{\Lambda}_v(\boldsymbol{q})^{-1} & \overline{\boldsymbol{\Lambda}}_{v\omega}(\boldsymbol{q}) \\ \overline{\boldsymbol{\Lambda}}_{v\omega}(\boldsymbol{q})^{\mathrm{T}} & \boldsymbol{\Lambda}_{\omega}(\boldsymbol{q})^{-1} \end{bmatrix}, \tag{69.6}$$

with $\overline{\boldsymbol{\Lambda}}_{v\omega}(\boldsymbol{q}) = \mathbf{J}_{\mathrm{c,lin}}(\boldsymbol{q})\mathbf{M}(\boldsymbol{q})^{-1}\mathbf{J}_{\mathrm{c,ang}}(\boldsymbol{q})^{\mathrm{T}}$. Finally, $m_{\boldsymbol{u}}$ is found to be

$$m_{\boldsymbol{u}} = [\boldsymbol{u}^{\mathrm{T}}\boldsymbol{\Lambda}_v(\boldsymbol{q})^{-1}\boldsymbol{u}]^{-1}. \tag{69.7}$$

It should be noted that the Jacobian has to be the *center-of-mass-Jacobian*. Otherwise, the entire inverse of the Cartesian inertia tensor has to be used, and not just its translational component block. More details can be found in [69.46]. We assume the local impact curvature in the $\boldsymbol{u}$-direction to be denoted by $c_{\boldsymbol{u}}$.

Haddadin, S., & Croft, E. (2016). Physical human–robot interaction. In *Springer Handbook of Robotics* (pp. 1835-1874). Springer, Cham.

Mass matrix examples - KUKA LBR iiwa

Run `ef_mass.m` demo.

Effective mass in downwards direction: 15.9604

X, Y, Z: 0.066, 0.000, 1.216

Mass matrix M:

0.315	-0.013	0.251	0.064	0.011	0.000	0.003
-0.013	6.515	0.007	-2.785	-0.110	0.431	0.000
0.251	0.007	0.683	0.054	-0.038	0.000	0.003
0.064	-2.785	0.054	1.643	0.058	-0.254	-0.000
0.011	-0.110	-0.038	0.058	0.040	0.001	0.003
0.000	0.431	0.000	-0.254	0.001	0.088	0.000
0.003	0.000	0.003	-0.000	0.003	0.000	0.003

End-effector mass matrix Λ:

0.202	-0.007	-0.020
-0.007	0.162	0.004
-0.020	0.004	0.063

Effective mass in downwards direction: 17.4501

X, Y, Z: 0.166, 0.000, 0.516

Mass matrix M:

0.417	0.114	0.343	-0.062	-0.059	0.000	0.003
0.114	1.675	0.125	-0.039	0.001	0.110	0.000
0.343	0.125	0.356	-0.064	-0.064	0.000	0.003
-0.062	-0.039	-0.064	0.991	0.059	0.072	-0.000
-0.059	0.001	-0.064	0.059	0.045	0.000	-0.003
0.000	0.110	0.000	0.072	0.000	0.088	0.000
0.003	0.000	0.003	-0.000	-0.003	0.000	0.003

End-effector mass matrix Λ:

0.199	0.010	0.024
0.010	0.127	0.021
0.024	0.021	0.057

Effective mass in downwards direction: 7.7501

X, Y, Z: 0.716, 0.000, 0.566

Mass matrix M:

5.099	0.050	1.503	-0.021	-0.320	0.000	0.003
0.050	5.571	0.017	-2.092	-0.100	0.133	0.000
1.503	0.017	0.674	0.044	-0.055	0.001	0.002
-0.021	-2.092	0.044	1.201	0.058	-0.033	-0.000
-0.320	-0.100	-0.055	0.058	0.099	0.000	-0.001
0.000	0.133	0.001	-0.033	0.000	0.088	0.000
0.003	0.000	0.002	-0.000	-0.001	0.000	0.003

End-effector mass matrix Λ:

0.189	0.002	0.011
0.002	0.180	0.019
0.011	0.019	0.129

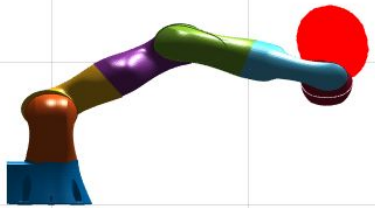

Mass matrix examples - UR10e

Effective mass in downwards direction: 5.4671

X, Y, Z: -0.050, -0.174, 0.546

Mass matrix M:

1.368	-0.719	0.244	-0.016	0.005	0.010
-0.719	1.804	-0.198	0.126	-0.000	-0.000
0.244	-0.198	1.784	-0.034	-0.000	-0.000
-0.016	0.126	-0.034	0.160	0.000	-0.000
0.005	-0.000	-0.000	0.000	0.016	0.000
0.010	-0.000	-0.000	-0.000	0.000	0.010

End-effector mass matrix Λ:

0.135	-0.001	-0.085
-0.001	0.867	-0.001
-0.085	-0.001	0.183

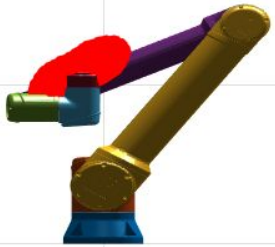

Run `ef_mass.m` demo: `ef_mass('robot','ur')`

Effective mass in downwards direction: 5.9076

X, Y, Z: 1.000, -0.174, 0.246

Mass matrix M:

7.848	-0.294	0.398	-0.016	-0.091	0.010
-0.294	7.262	2.817	0.450	0.000	-0.000
0.398	2.817	2.356	0.253	0.000	-0.000
-0.016	0.450	0.253	0.160	0.000	-0.000
-0.091	0.000	0.000	0.000	0.016	0.000
0.010	-0.000	-0.000	-0.000	0.000	0.010

End-effector mass matrix Λ:

0.223	0.000	-0.030
0.000	0.881	-0.001
-0.030	-0.001	0.169

Effective mass for pHRI

Can be considered in:

1. robot design
    a. Lee, S. D., Kim, B. S., & Song, J. B. (2013). Human–robot collision model with effective mass and manipulability for design of a spatial manipulator. *Advanced Robotics*, 27(3), 189-198.
2. application design - where in the workspace and in which direction collisions can occur

3D Collision Force Map - case study

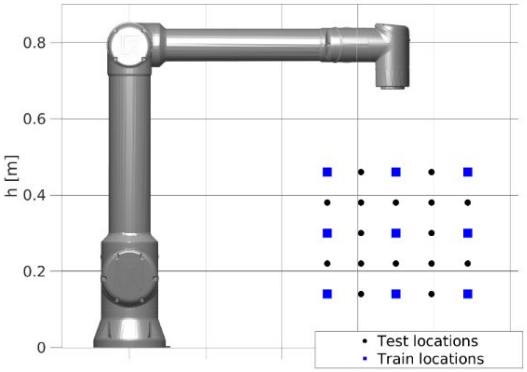

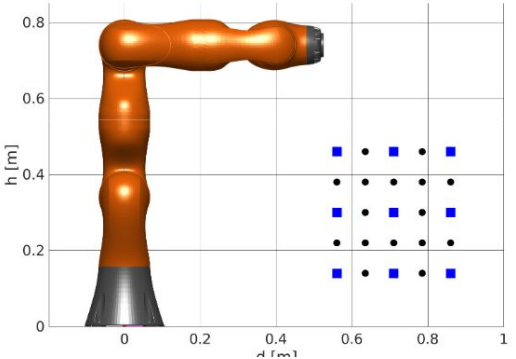

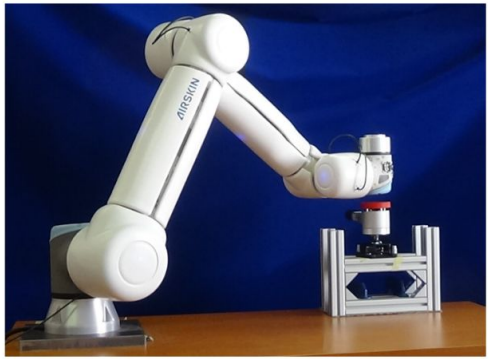

(a) UR10e.

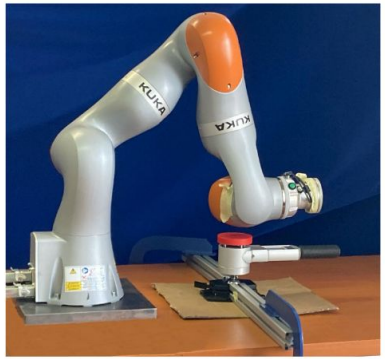

(b) KUKA LBR iiwa.

Fig. 1: Setup – robots and impact measuring device.

dataset	samples per state	training states (used samples*)	testing states (used samples*)
UR10e	3	27 (75)	88 (249)
KUKA 30 Nm	3	27 (78)	98 (291)
KUKA 10 Nm	1	27 (26)	98 (98)

Svarny, P., Rozlivek, J., Rustler, L., & Hoffmann, M. (2021, May). 3D Collision-Force-Map for Safe Human-Robot Collaboration. In *2021 IEEE International Conference on Robotics and Automation (ICRA)* (pp. 3829-3835). IEEE.

ISO/TS 15066 predictions

from TS 15066 relating velocity (v) and (maximum) impact force ($F_{\max}$) is:

$$v \leq \frac{F_{\max}}{\sqrt{k}} \sqrt{m_R^{-1} + m_H^{-1}}, \quad (1)$$

with m_R the effective robot mass, m_H the human body part mass, k the spring constant for the human body part and $F_{\max}$ the maximum impact force permitted for the given body region. As pointed out in [6], this is a simplified contact model with a single spring constant for the human body.

$$\mathcal{F}_{\text{ext}}^{\max} = \sqrt{\frac{m_u M_{\text{H}}}{m_u + M_{\text{H}}}} \sqrt{K_{\text{H}}} \dot{x}_{\text{re}}^{0}$$

Position in workspace and collision direction not considered!

If we investigate constrained dynamic impacts, even without clamping, we can approximate $m_H^{-1} \approx 0$ as in [7][1]. This approximation allows us also to simplify the situation by investigating the relative velocity as simply the robot velocity with the human hand being still. The other variables are therefore set based on [4] as $F_{\max} = 140$ N and $k = 75000$ N/m. The moving masses of the UR and KUKA robot are approximately 30 kg and 20 kg respectively. Using the approximation from [4] that the effective robot mass m_R is $M/2 + m_L$ (half of the total mass of the moving parts of the robot, plus the effective payload m_L, which is zero in our case), together with Eq. 1, would give permissible velocity up to 0.13 m/s for the UR robot and 0.16 m/s for the KUKA robot in case of clamping. If there is no clamping, the permissible force becomes 280 N and thus also the velocities are higher, namely 0.26 m/s for the UR and 0.32 m/s for the KUKA due to the weight difference between the robots.

Svarny, P., Rozlivek, J., Rustler, L., & Hoffmann, M. (2021, May). 3D Collision-Force-Map for Safe Human-Robot Collaboration. In *2021 IEEE International Conference on Robotics and Automation (ICRA)* (pp. 3829-3835). IEEE.

3D Collision Force Map - case study

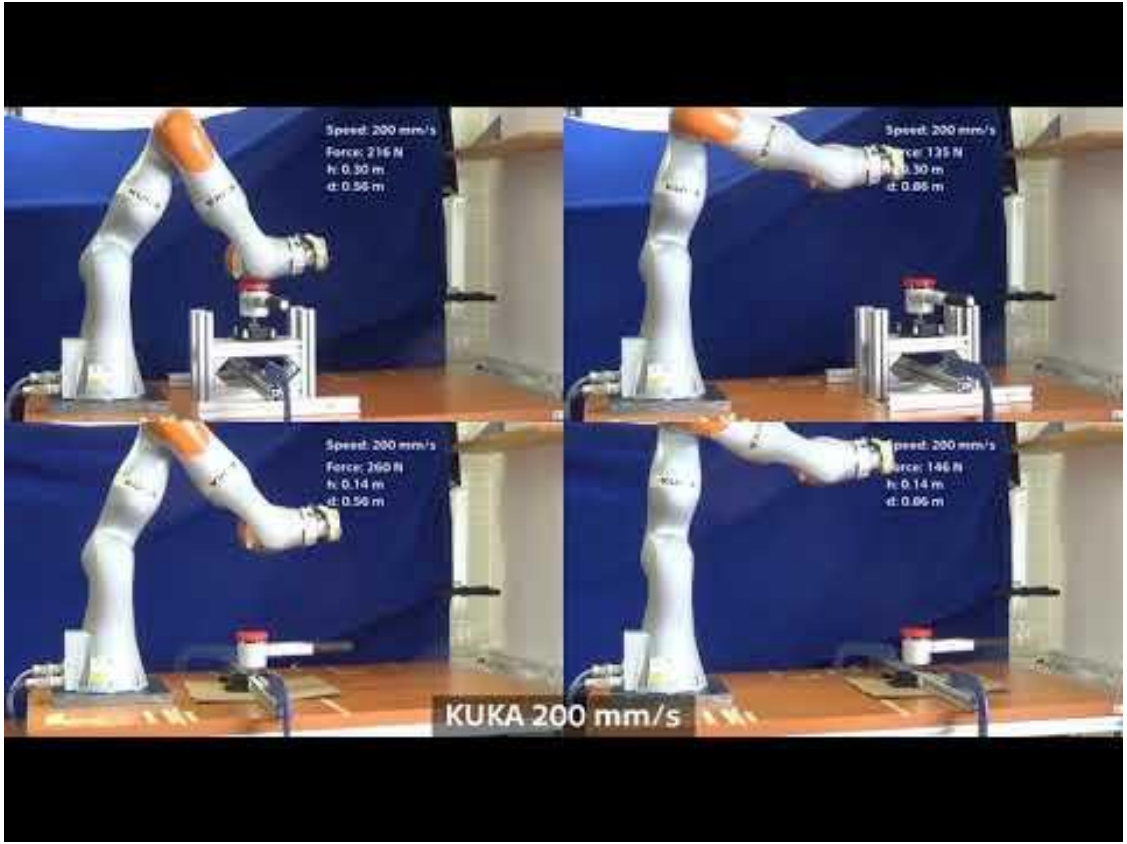

Svarny, P., Rozlivek, J., Rustler, L., & Hoffmann, M. (2021, May). 3D Collision-Force-Map for Safe Human-Robot Collaboration. In *2021 IEEE International Conference on Robotics and Automation (ICRA)* (pp. 3829-3835). IEEE.

3D CFM case study - measurements

$$\mathcal{F}_{\text{ext}}^{\max} = \sqrt{\frac{m_u M_{\text{H}}}{m_u + M_{\text{H}}}} \sqrt{K_{\text{H}}} \dot{x}_{\text{re}}^{0}$$

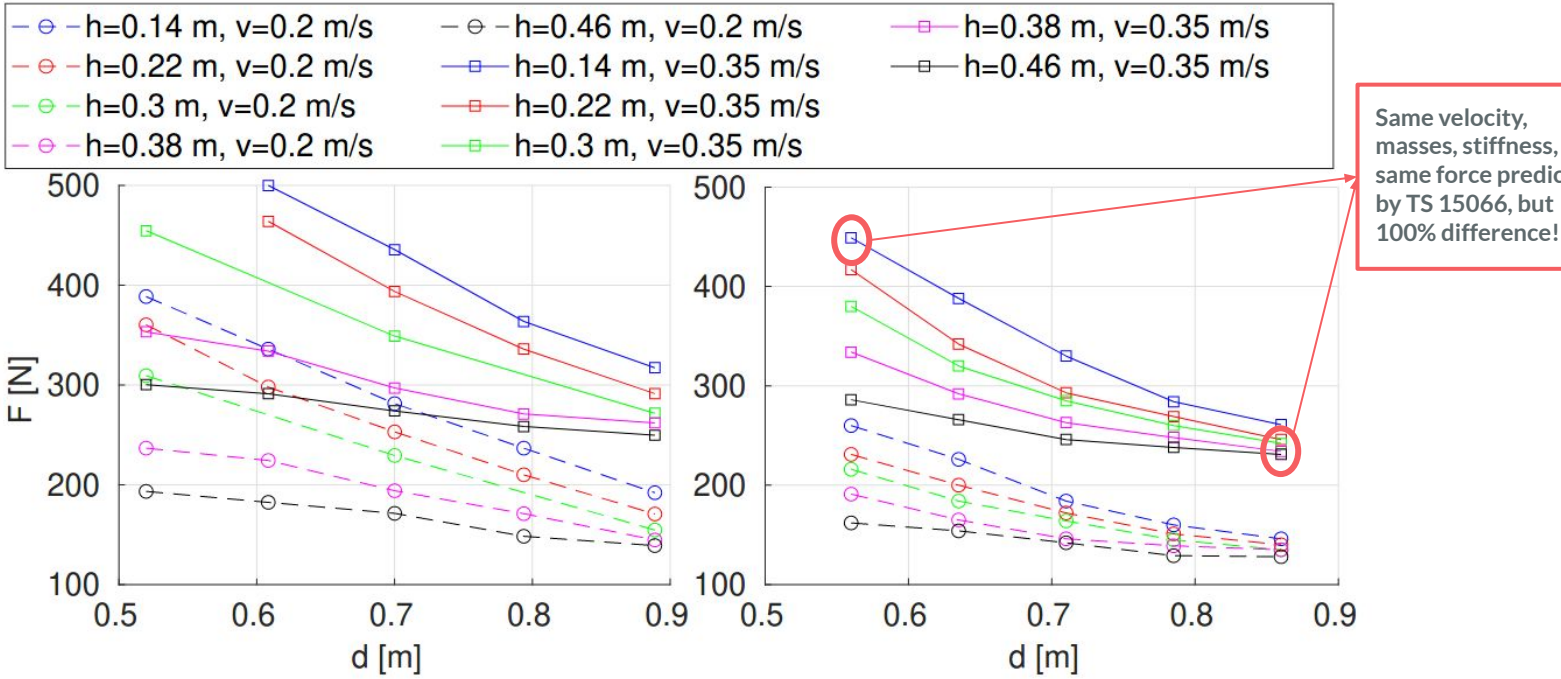

collision direction down

UR10e

KUKA lbr iiwa

Svarny, P., Rozlivek, J., Rustler, L., & Hoffmann, M. (2021, May). 3D Collision-Force-Map for Safe Human-Robot Collaboration. In *2021 IEEE International Conference on Robotics and Automation (ICRA)* (pp. 3829-3835). IEEE.

3D CFM – predicting impact force

$$\ln(F) = \beta_0 + \beta_1 \cdot v + \beta_2 \cdot d + \beta_3 \cdot d^2 + \beta_4 \cdot d \cdot h + \\ + \beta_5 \cdot h^2 + \beta_6 \cdot d^2 \cdot v + \beta_7 \cdot d \cdot v^2 + \beta_8 \cdot d \cdot h^2$$

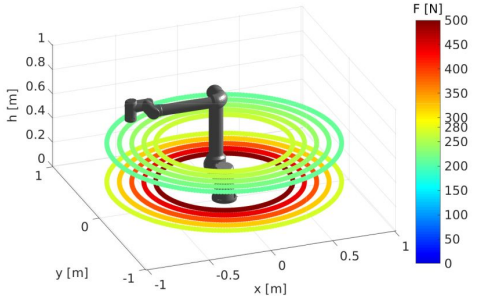

Fig. 6: UR10e – concentric impact force circles at various heights for end effector speed of 350 mm/s. Plotted are values from the 3D CFM model.

Svarny, P., Rozlivek, J., Rustler, L., & Hoffmann, M. (2021, May). 3D Collision-Force-Map for Safe Human-Robot Collaboration. In *2021 IEEE International Conference on Robotics and Automation (ICRA)* (pp. 3829-3835). IEEE.

end effector velocity 0.30 m/s (direction down)

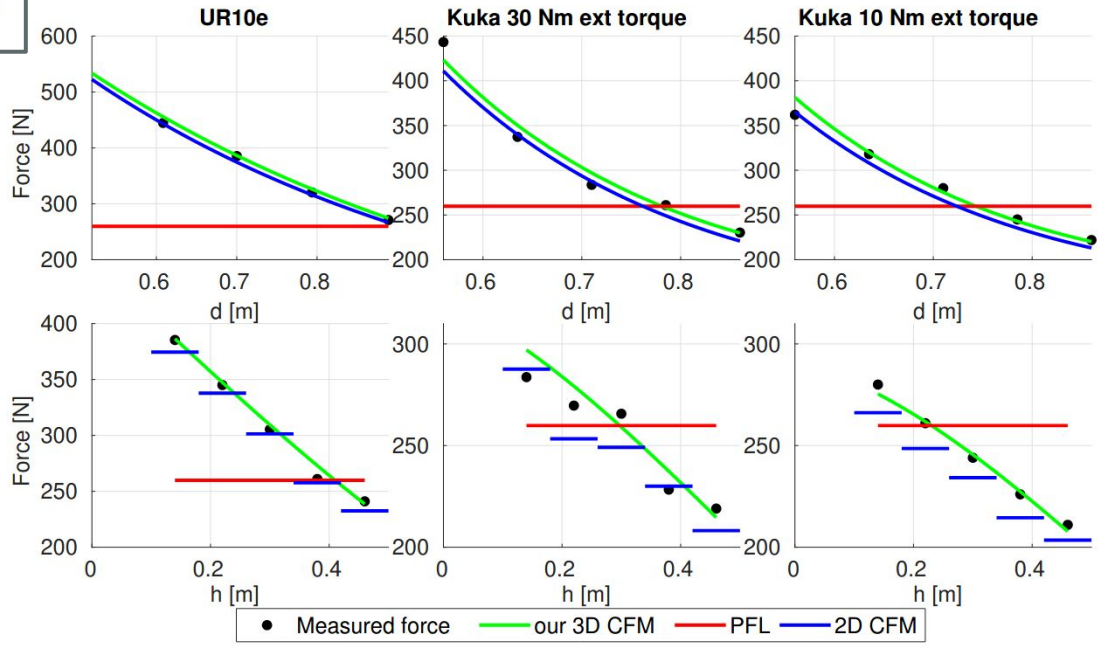

2D CFM - A. Schlotzhauer, L. Kaiser, J. Wachter, M. Brandstötter, and M. Hofbaur, "On the trustability of the safety measures of collaborative robots: 2D Collision-force-map of a sensitive manipulator for safe HRC," in 2019 IEEE 15th International Conference on Automation Science and Engineering (CASE). IEEE, 2019, pp. 1676–1683.

3D CFM case study - need for in situ measurement

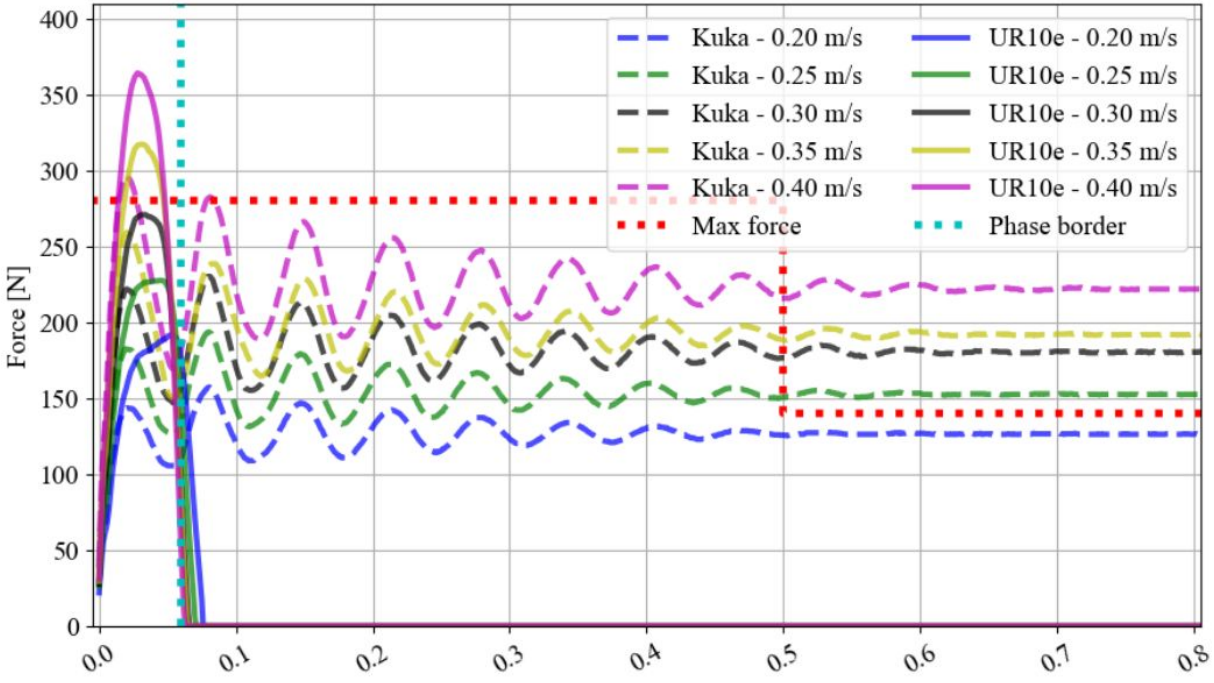

Svarny, P., Rozlivek, J., Rustler, L., & Hoffmann, M. (2021, May). 3D Collision-Force-Map for Safe Human-Robot Collaboration. In *2021 IEEE International Conference on Robotics and Automation (ICRA)* (pp. 3829-3835). IEEE.

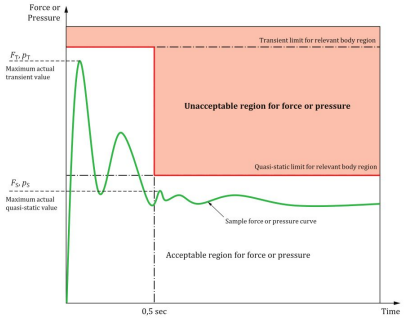

Figure 4 — Graphical representation of acceptable and unacceptable forces or pressures

ISO/TS 15066:2016
Robots and robotic devices — Collaborative robots

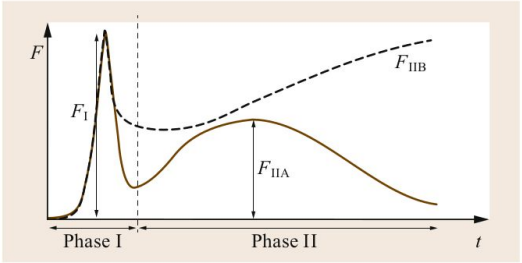

Fig. 69.6 Typical robot–human collision force profiles

Haddadin, S., & Croft, E. (2016). Physical human–robot interaction. In *Springer handbook of robotics* (pp. 1835-1874). Springer, Cham.

See also:

Proceedings of the 2021 IEEE International
Conference on Intelligence and Safety for Robotics
Nagoya, Japan, March 4-6, 2021

Notion on the Correct Use of the Robot Effective Mass in the Safety Context and Comments on ISO/TS 15066

Robin Jeanne Kirschner, Nico Mansfeld, Guillermo Gómez Peña, Saeed Abdolshah and Sami Haddadin

***Abstract*— Collision experiments in the human-robot interaction (HRI) context showed that the effective robot mass is one of the main parameters that influence human injury probability during a collision. Also the current standard ISO/TS 15066 highlights the importance of this parameter and provides a method to determine the maximum safe robot velocity based on the effective mass. To enable both safe and efficient robot applications, it is crucial to derive the robot's instantaneous effective mass sufficiently accurate based on either a), a kinematic and dynamic model or b), a suitable collision experiment. In this paper, we describe and quantitatively compare the well-established reflected mass model by Khatib and the simplified model provided in the ISO/TS 15066 for the KUKA LWR IV+ and the Franka Emika Panda robot. Furthermore, we propose a method to practically determine the effective mass using a passive mechanical pendulum setup. Our results show that the simplified ISO/TS model can lead to a significant safety-relevant error. With our preliminary experimental setup, however, we can verify that the reflected mass obtained by the dynamics model only differs $1.1-7.8\,\%$ from the measured value.**

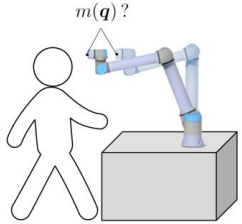

Fig. 1. The robot effective mass is a crucial parameter for safety assessment and safe control in HRI.

the ISO/TS, respectively [10], it is important to determine the

Kirschner, R. J., Mansfeld, N., Peña, G. G., Abdolshah, S., & Haddadin, S. (2021, March). Notion on the Correct Use of the Robot Effective Mass in the Safety Context and Comments on ISO/TS 15066. In *2021 IEEE International Conference on Intelligence and Safety for Robotics (ISR)* (pp. 6-9). IEEE.

Missing piece - effective mass and empirical model

Analysis of the maximum permissible velocities in PFL regime.

- Collect data from robot collisions with the measuring device.
- Analyze them to find a simplified relation between robot speed and collision force (e.g., polynomial fitting).
- Analyze the influence of effective mass on the collision force.
- We did only collision direction down so far.

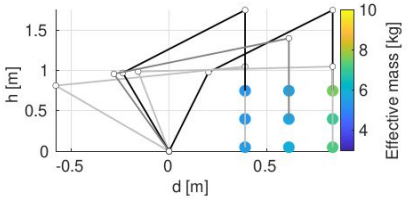

(a) m_R at 9 inspection points.

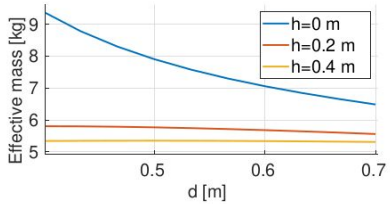

(b) m_R as a function of d and h.

Fig. 4: Calculating effective mass of model 3 DoF planar manipulator. Collision direction "down": $u = [0, -1]$.

Factors affecting safety in the PFL regime

- Robot velocity
  - constraints: cycle time of the application
- Robot effective mass
  - How can you reduce it?
    - lightweight design
    - **position in workspace**
- Impactors
  - shape
  - stiffness
- Collision reaction
  - safety stop categories
  - *interaction control*

Airskin case study

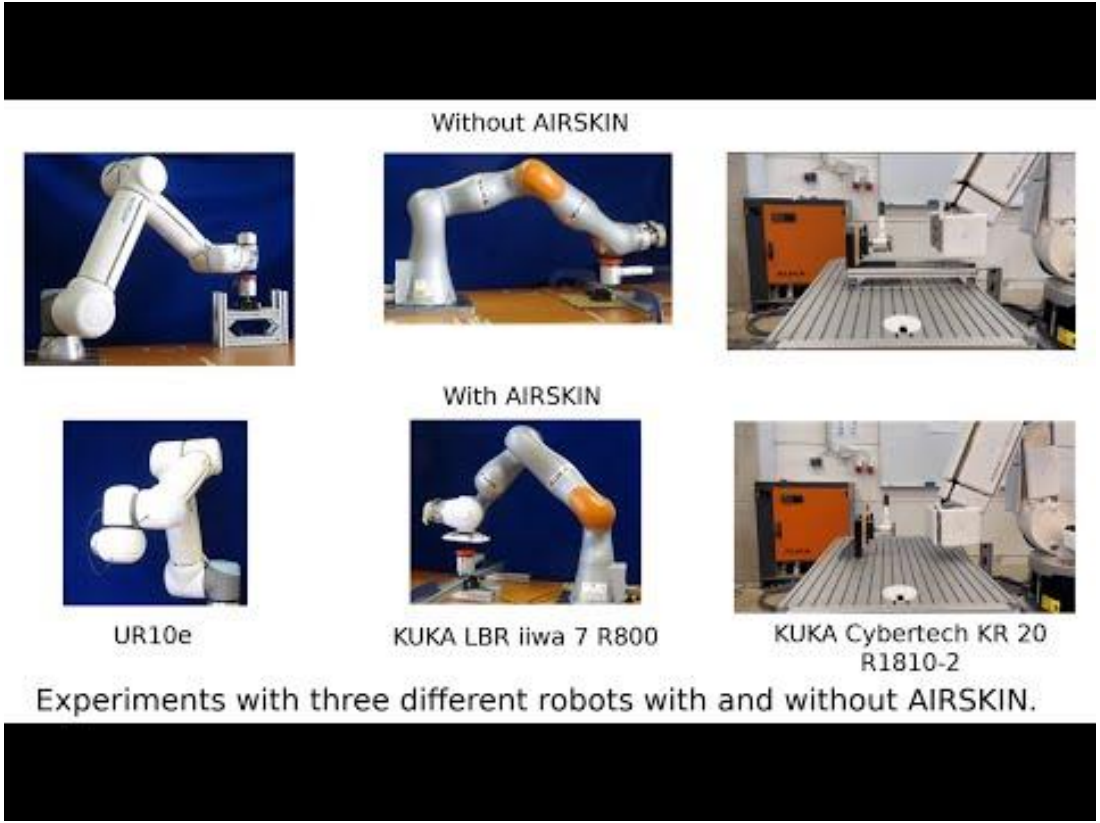

Svarny, P., Rozlivek, J., Rustler, L., Sramek, M., Deli, Ö., Zillich, M. and Hoffmann, M. (2022), 'Effect of active and passive protective soft skins on collision forces in human–robot collaboration', *Robotics and Computer-Integrated Manufacturing* **78**, 102363.

Airskin case study - setup

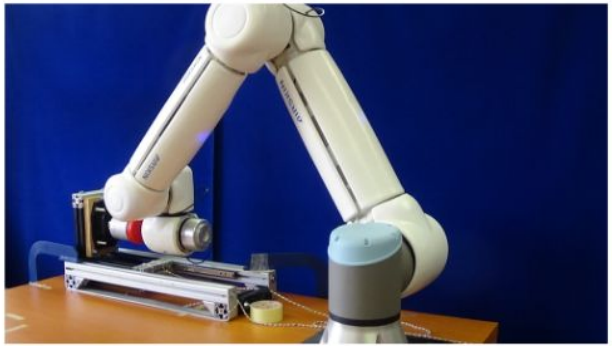

(a) UR10e with AIRSKIN (transient contact).

(b) KUKA iiwa with AIRSKIN module pad (quasi-static contact).

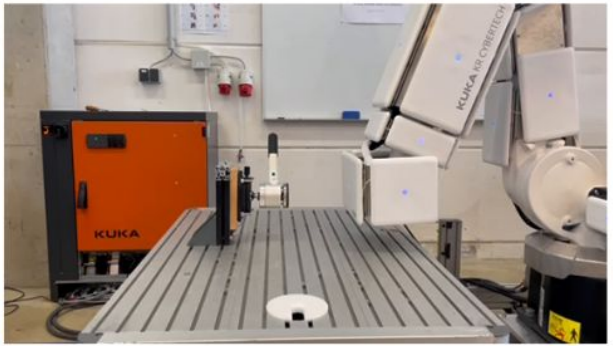

(c) KUKA Cybertech with AIRSKIN module pad (quasi-static contact).

Robot	Safety	Values		
UR10e	Preset	Pre-2	Pre-4	
	Skin	E-Stop	S-Stop	
KUKA iiwa	External torque	Stop 0	Stop 1	Stop 1 op
	Skin	Stop 0	Stop 1	Stop 1 op
KUKA Cybertech	Skin	Stop 1 op	Stop 2	

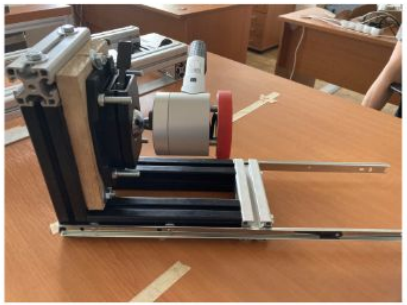

(a) Moving mass

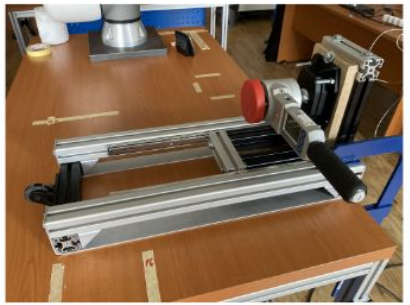

(b) Whole construction

Figure 3: Transient contact simulation construction.

Svarny, P., Rozlivek, J., Rustler, L., Sramek, M., Deli, Ö., Zillich, M. and Hoffmann, M. (2022), 'Effect of active and passive protective soft skins on collision forces in human–robot collaboration', *Robotics and Computer-Integrated Manufacturing* **78**, 102363.

Airskin case study - positions and impact directions

Type	#	direction vector	UR10e	KUKA iiwa	KUKA Cybertech
quasi-static	0	$\begin{pmatrix}0\\0\\-1\end{pmatrix}$	0.85 0.27 0.14	0.66 0.00 0.14	–
	1	$\begin{pmatrix}0\\1\\0\end{pmatrix}$	0.79 0.14 0.16	0.35 0.14 0.16	0.00 0.90 0.18
	2	$\begin{pmatrix}1\\0\\0\end{pmatrix}$	0.80 −0.22 0.16	0.37 −0.31 0.16	0.25 0.75 0.18
transient	3	$\begin{pmatrix}0\\1\\0\end{pmatrix}$	0.79 0.18 0.16	0.35 0.10 0.16	0.00 0.90 0.18
	4	$\begin{pmatrix}1\\0\\0\end{pmatrix}$	0.82 −0.22 0.16	0.33 −0.31 0.16	0.25 0.75 0.18

Table 3: World frame coordinates for the impact locations. The number # identifies the place, the direction vector is given in the world frame and the coordinates are given in the world frame. The origin of the world frame is located at the base frame of the robot.

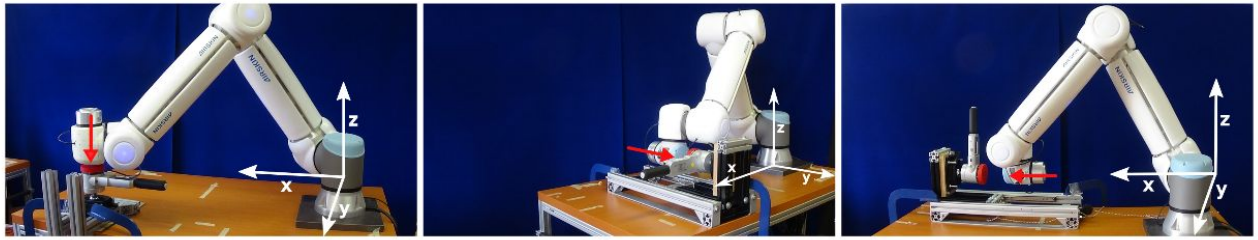

(a) Impact direction downward ([0, 0, −1]), quasi-static case (b) Impact direction along the y-axis ([0, 1, 0]), transient case (c) Impact direction along the x-axis ([1, 0, 0]), transient case

Figure 5: Impact directions. The origin of the world reference frame is always at the base frame of the robot. The coordinates in the image are moved for visibility.

Svarny, P., Rozlivek, J., Rustler, L., Sramek, M., Deli, Ö., Zillich, M. and Hoffmann, M. (2022), 'Effect of active and passive protective soft skins on collision forces in human–robot collaboration', *Robotics and Computer-Integrated Manufacturing* **78**, 102363.

Emergency stop categories

Stop Categories according to IEC 60204-1 (NFPA79). Only Category 0 and 1 stops are allowed for the Estop.

- **Category 0 & 1** result in the removal of drive power, with Cat 0 being IMMEDIATE & Cat 1 being a controlled stop (decelerate then removal). With all UR robots, a Category 1 stop is a controlled stop where power is removed when a monitored standstill state is detected.
- **Category 2** is a stop where drive power is NOT removed. For Category 2 stops, this specification is defined in IEC 60204-1, A description of STO, SS1 and SS2 in IEC 61800-5-2.
  With UR robots, a Category 2 stop maintains the trajectory then retains power to the drives after stopping.

Any limit violation, or fault detected in a safety function, results in a Category 0 stop.

SF #	Safety Function	Description	PFHd	What is controlled
1	**Emergency Stop** 1, 2, 3	Pressing the Estop PB on the pendant[1] or the External Estop (if using the Estop Safety Input) results in a Cat 1 stop[3]. Command[1] all joints to stop and upon all joints coming to a monitored standstill state, power is removed. This is a Cat 1 stop[3]. See Stop Time and Stop Distance Safety Functions[4] and the User Manual.	**1.30E-07**	**Robot**
2	**Safeguard Stop** (Protective Stop according to ISO 10218-1)	This safety function is initiated by an external protective device using safety inputs which will initiate a Cat 2 stop[3]. See the Stop Time and Stop Distance Safety Functions[4] and the User Manual. *For the functional safety of the complete integrated safety function, add the PFHd of the external protective device to the PFHd of the Safeguard Stop.*	**1.20E-07**	**Robot**

UR e-Series Safety Functions and Safety I/O

UNIVERSAL ROBOTS

Slide from Alessandro de Luca: Physical HRI. http://www.diag.uniroma1.it/deluca/pHRI_elective/pHRI_SafetyDependability.pdf

Airskin case study - collision forces

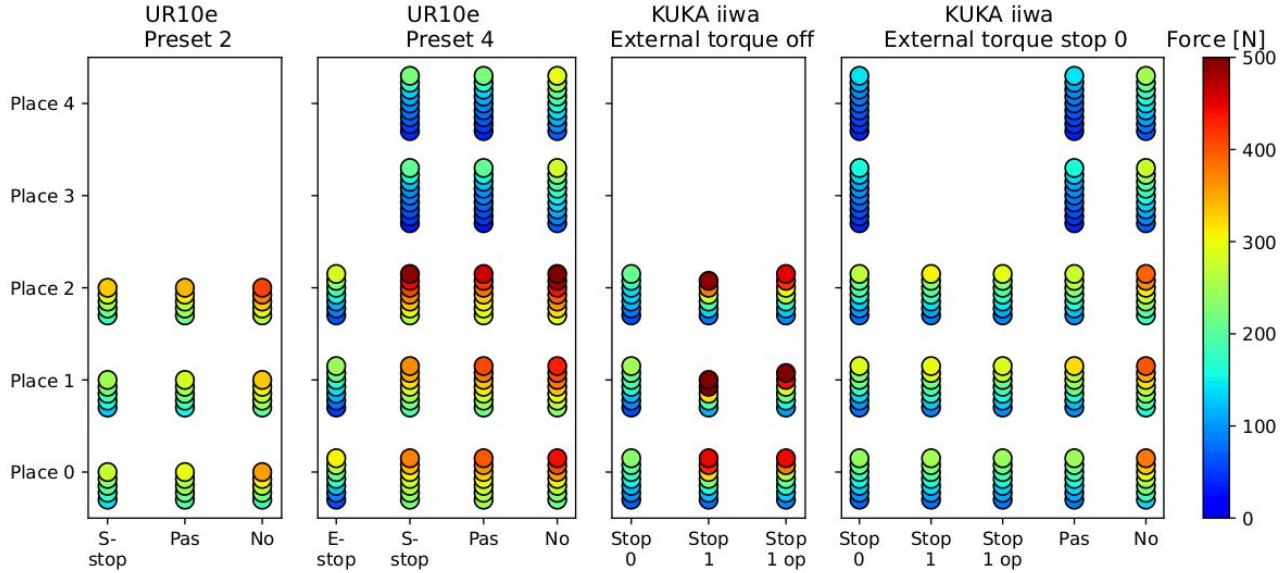

Figure 11: Peak impact forces comparison for the various UR10e and KUKA iiwa with various external torque settings. The circles represent the measured 7 velocities (from 0.2 to 0.5 m/s with increment 0.05 m/s), where applicable. The initiated stop behavior is either a Stop 0, Stop 1, or Stop 1 op on KUKA iiwa. For UR10e, these stops were Safeguard stop (S-stop) and Emergency stop (E-stop) and also the safety preset was considered (Pre-2 or Pre-4). The 'Pas' in the case of the AIRSKIN means the pads are pressurized but they do not initiate a stop, while 'No' means the AIRSKIN pad was removed from the robot. The three locations Place 0, 1, 2 are quasi-static collisions in the three directions downward, along y-axis, along x-axis respectively. The transient collisions along y-axis and along x-axis are Place 3, 4 respectively.

Place			Coordinates [m]		
Type	#	direction vector	UR10e	KUKA iiwa	KUKA Cybertech
quasi-static	0	$\begin{pmatrix}0\\0\\-1\end{pmatrix}$	0.85 0.27 0.14	0.66 0.00 0.14	–
	1	$\begin{pmatrix}0\\1\\0\end{pmatrix}$	0.79 0.14 0.16	0.35 0.14 0.16	0.00 0.90 0.18
	2	$\begin{pmatrix}1\\0\\0\end{pmatrix}$	0.80 −0.22 0.16	0.37 −0.31 0.16	0.25 0.75 0.18
transient	3	$\begin{pmatrix}0\\1\\0\end{pmatrix}$	0.79 0.18 0.16	0.35 0.10 0.16	0.00 0.90 0.18
	4	$\begin{pmatrix}1\\0\\0\end{pmatrix}$	0.82 −0.22 0.16	0.33 −0.31 0.16	0.25 0.75 0.18

Table 3: World frame coordinates for the impact locations. The number # identifies the place, the direction vector is given in the world frame and the coordinates are given in the world frame. The origin of the world frame is located at the base frame of the robot.

Svarny, P., Rozlivek, J., Rustler, L., Sramek, M., Deli, Ö., Zillich, M. and Hoffmann, M. (2022), 'Effect of active and passive protective soft skins on collision forces in human–robot collaboration', *Robotics and Computer-Integrated Manufacturing* **78**, 102363.

Airskin case study - force evolution after impact

quasi-static contact,
0.3 m/s, place 2
KUKA iiwa, UR10e

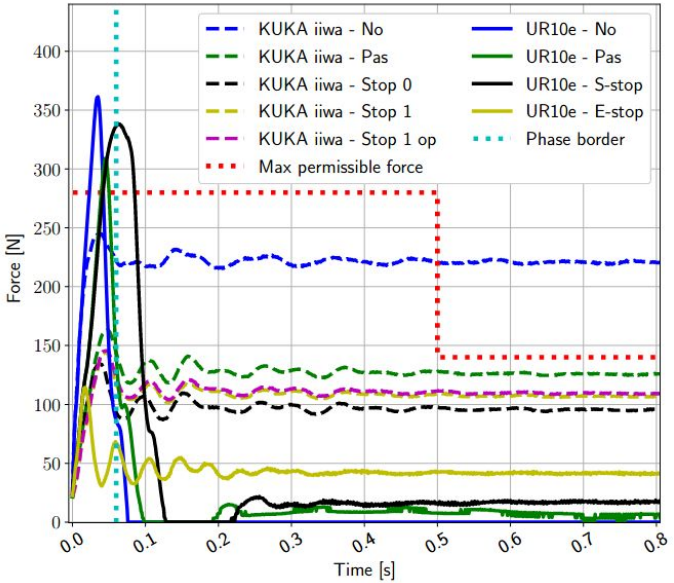

theory

ISO/TS 15066:2016 Robots and robotic devices — Collaborative robots

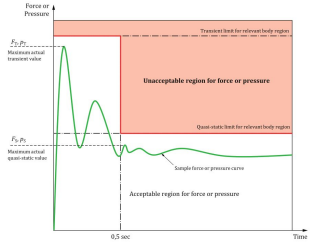

Figure 4 — Graphical representation of acceptable and unacceptable forces or pressures

Haddadin, S., & Croft, E. (2016). Physical human–robot interaction. In *Springer handbook of robotics* (pp. 1835-1874). Springer, Cham.

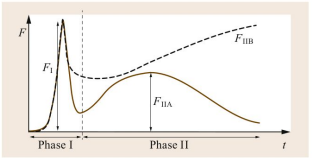

Fig. 69.6 Typical robot–human collision force profiles

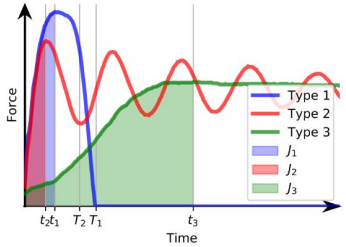

KUKA Cybertech

quasi-static

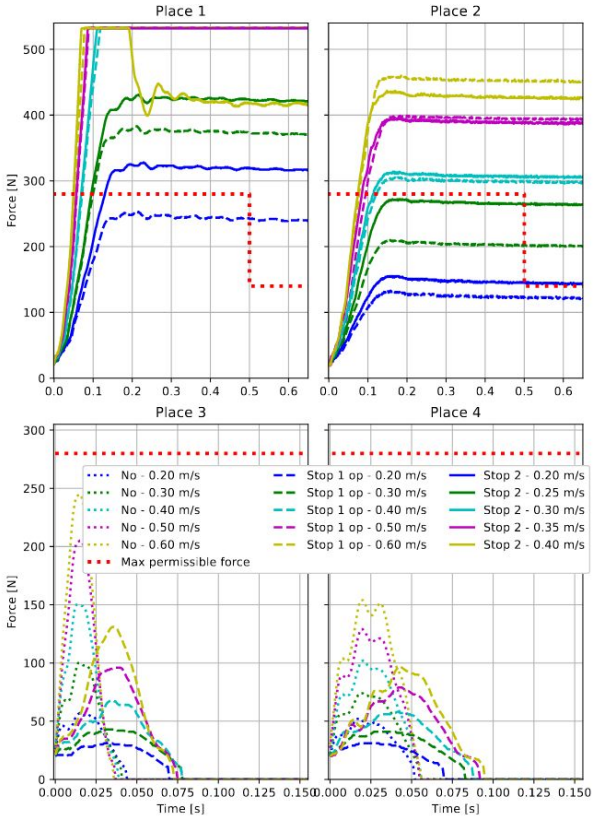

transient

Svarny, P., Rozlivek, J., Rustler, L., Sramek, M., Deli, Ö., Zillich, M. and Hoffmann, M. (2022), 'Effect of active and passive protective soft skins on collision forces in human–robot collaboration', *Robotics and Computer-Integrated Manufacturing* **78**, 102363.

Airskin case study - KUKA iiwa - stop types

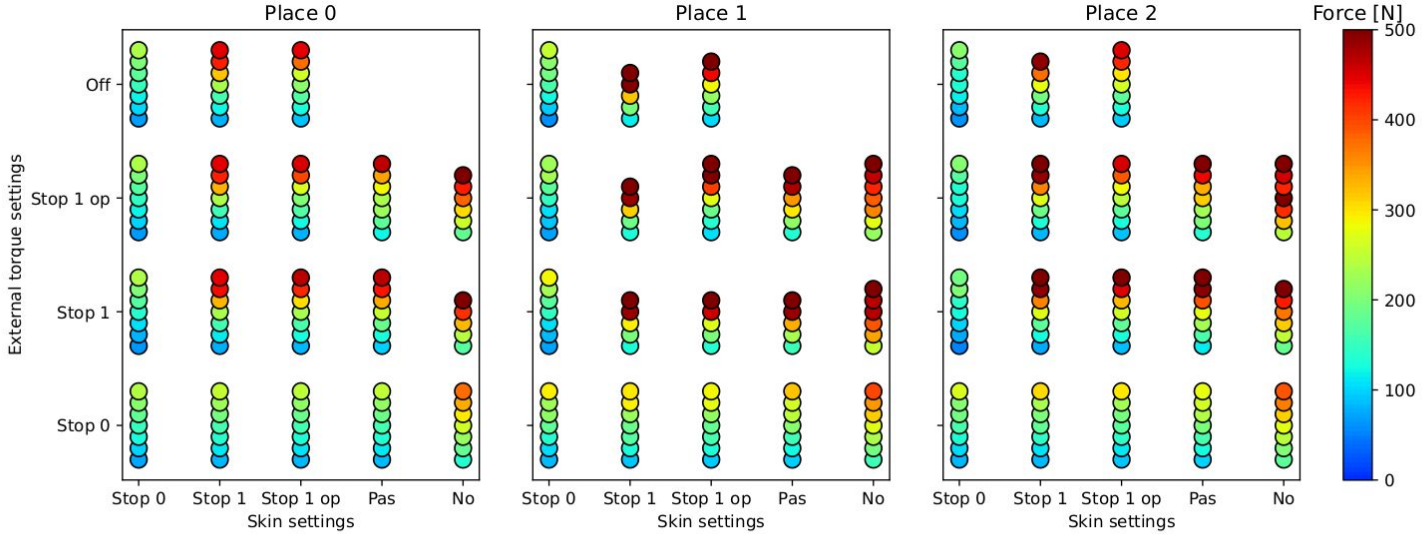

Figure 12: KUKA iiwa various stop combinations for quasi-static impacts. The initiated stop behavior is either a category 0 stop (Stop 0), a category 1 stop (Stop 1), a category 1 stop on path (Stop 1 op). The 'Pas' in the case of the AIRSKIN means the pads are pressurized but they do not initiate a stop, while 'No' means the AIRSKIN pad was removed from the robot. The 'Off' setting for the torques means that they were turned off. The circles represent the measured 7 velocities (from 0.2 to 0.5 m/s with increment 0.05 m/s), where applicable. The three locations Place 0, 1, 2 are downward, along y-axis, along x-axis respectively.

Svarny, P., Rozlivek, J., Rustler, L., Sramek, M., Deli, Ö., Zillich, M. and Hoffmann, M. (2022), 'Effect of active and passive protective soft skins on collision forces in human–robot collaboration', *Robotics and Computer-Integrated Manufacturing* **78**, 102363.

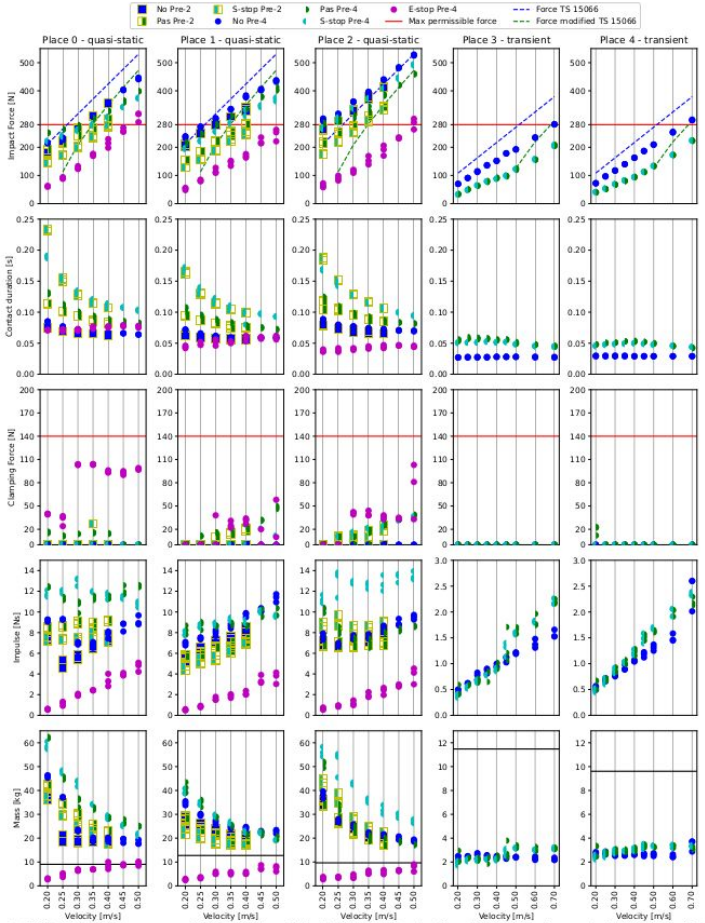

Figure 7: UR10e summary of measurements. The AIRSKIN module is either absent (No), active (S-stop/E-stop) or merely pressurized but not active (Pas). The robot is either in the least restrictive preset (Pre-4) or in the second most restrictive preset (Pre-2). In addition, active skin could trigger either the safeguard stop (S-stop) or the emergency stop (E-stop). The duration is the time between the impact detection and the first local minimum of the force measurement, i.e., the end of Phase I. The maximum permissible force is derived from TS 15066. Dashed lines are force predictions from Eq. 7 – see Sec. 2.4. The effective mass is calculated from the UR10e model.

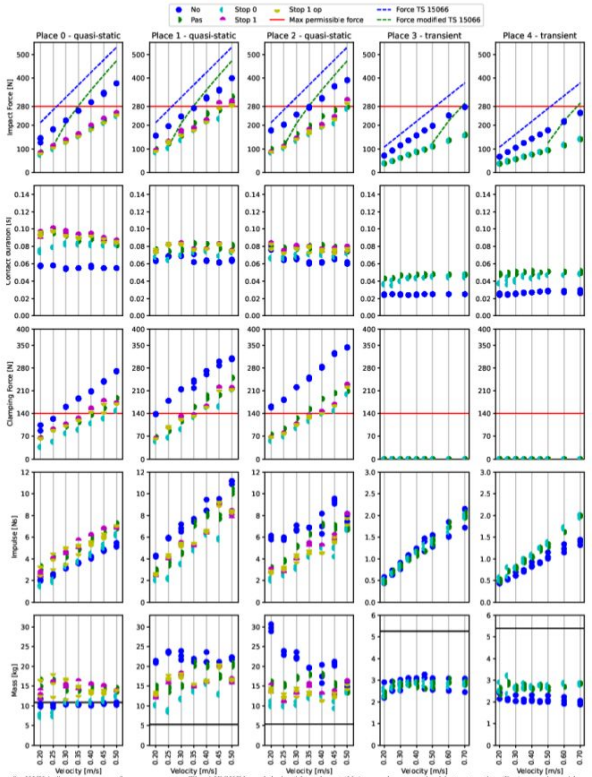

Figure 9: KUKA iiwa summary of measurements. The AIRSKIN module is either absent (No), merely pressurized but not active (Pas) or active with various stopping behaviors (Stop 0, Stop 1, Stop 1 op). The maximum permissible force is derived from TS 15066. Dashed lines are force predictions from Eq. 7 – see Sec. 2.4. The duration is the time between the impact detection and the first local minimum of the force measurement, i.e., the end of Phase I. The effective mass is calculated from the KUKA iiwa model.

Svarny, P., Rozlivek, J., Rustler, L., Sramek, M., Deli, Ö., Zillich, M. and Hoffmann, M. (2022), 'Effect of active and passive protective soft skins on collision forces in human–robot collaboration', *Robotics and Computer-Integrated Manufacturing* **78**, 102363.

Airskin case study - pad stiffness

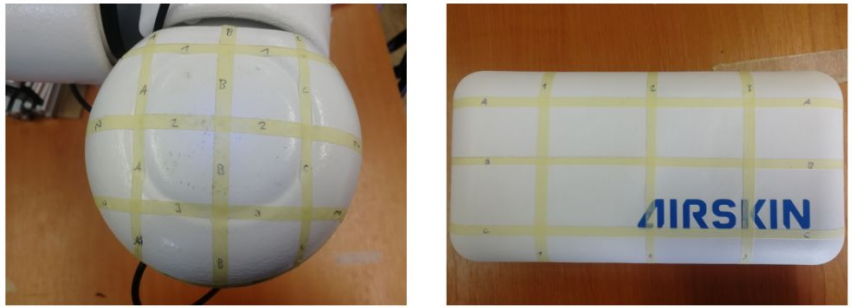

(a) UR-skin (b) The Pad

Figure 4: AIRSKIN pads with measurement grid.

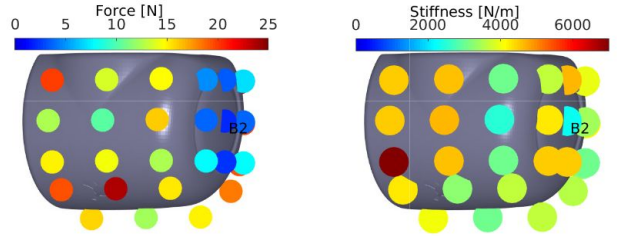

Figure 13: UR-skin threshold force (left) and stiffness (right). The measured values are color-coded. The impact point, B2, is also marked.

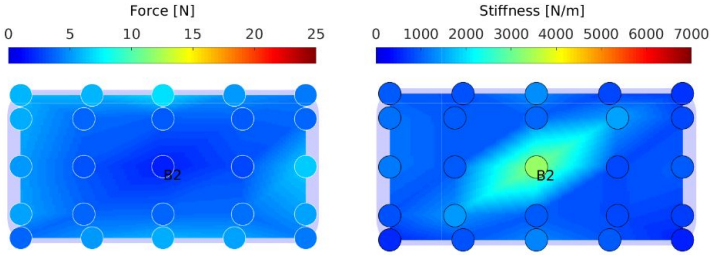

Figure 14: The Pad threshold force (left) and stiffness (right). The measured values are color-coded. The impact point, B2, is also marked.

Svarny, P., Rozlivek, J., Rustler, L., Sramek, M., Deli, Ö., Zillich, M. and Hoffmann, M. (2022), 'Effect of active and passive protective soft skins on collision forces in human–robot collaboration', *Robotics and Computer-Integrated Manufacturing* **78**, 102363.

Airskin case study - soft cover model

ISO/TS 15066

$$v \leq \frac{F_{\max}}{\sqrt{k}} \sqrt{m_R^{-1} + m_H^{-1}} = \frac{F_{\max}}{\sqrt{k \cdot \mu}},$$

Soft cover model

$$v \leq \sqrt{\frac{F_{\max}^2}{k \cdot \mu} + \frac{d_s^2 \cdot k_s}{\mu}}$$

Svarny, P., Rozlivek, J., Rustler, L., Sramek, M., Deli, Ö., Zillich, M. and Hoffmann, M. (2022), 'Effect of active and passive protective soft skins on collision forces in human–robot collaboration', *Robotics and Computer-Integrated Manufacturing* **78**, 102363.

Airskin case study – soft cover model results

UR10e

KUKA iiwa

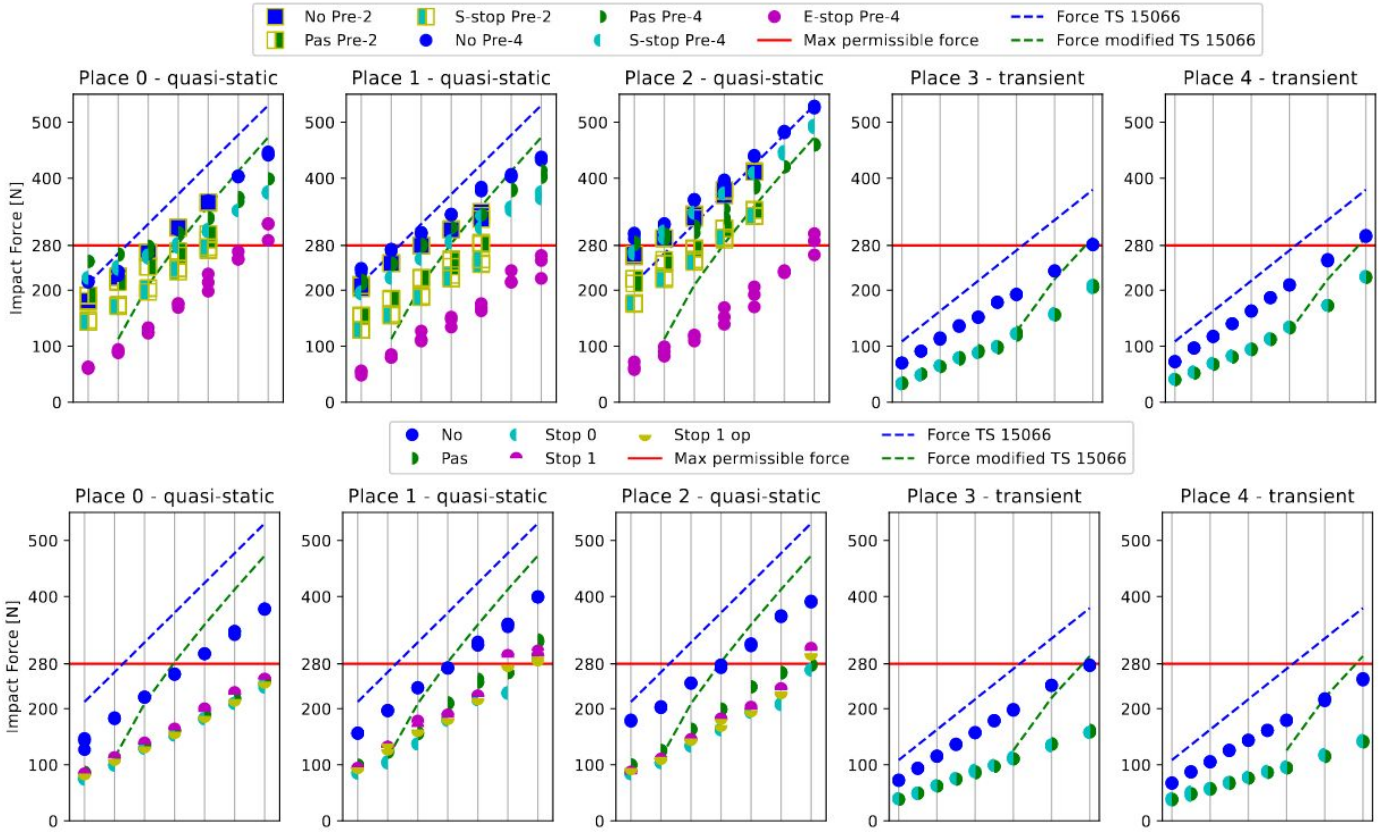

Svarny, P., Rozlivek, J., Rustler, L., Sramek, M., Deli, Ö., Zillich, M. and Hoffmann, M. (2022), 'Effect of active and passive protective soft skins on collision forces in human–robot collaboration', *Robotics and Computer-Integrated Manufacturing* **78**, 102363.

Factors affecting safety in the PFL regime

- Robot velocity
  - constraints: cycle time of the application
- Robot effective mass
  - How can you reduce it?
    - lightweight design
    - position in workspace and impact directions
- Impactors
  - shape
  - stiffness
- Collision reaction
  - safety stop categories
  - interaction control

Factors affecting safety in the PFL regime

- Robot velocity
  - constraints: cycle time of the application
- Robot effective mass
  - How can you reduce it?
    - lightweight design
    - **position in workspace and impact directions**
- Impactors
  - shape
  - **stiffness**
- Collision reaction
  - **safety stop categories**
  - *interaction control*

Robot collisions - detection, ..., reaction

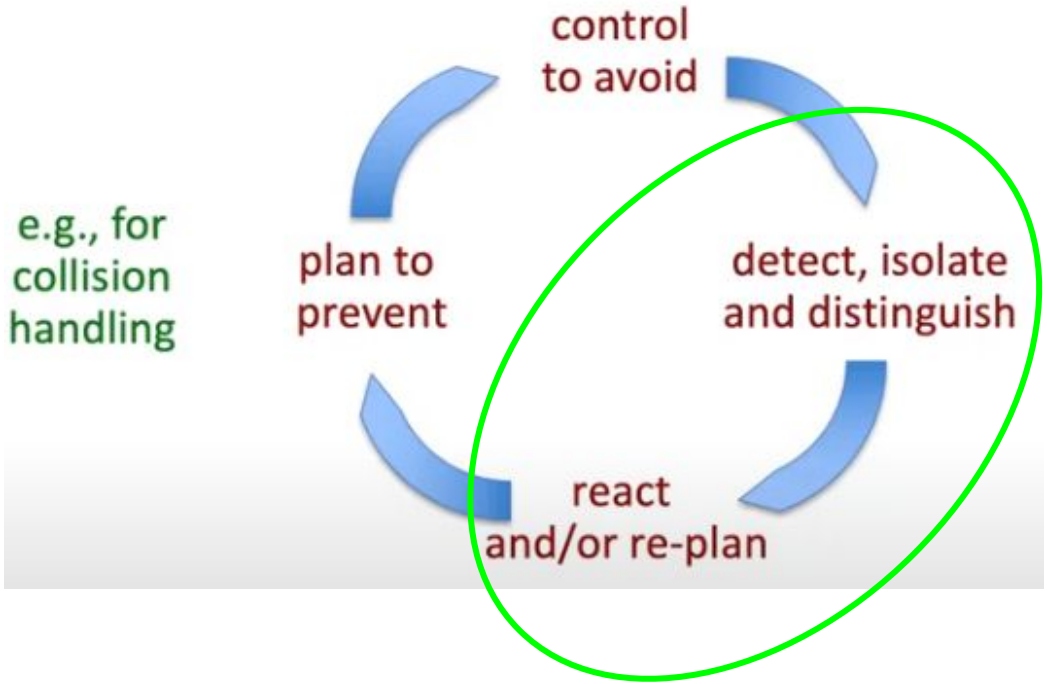

Alessandro de Luca, From Human-Robot Interaction to Collaborative Control: A Human Centered Perspective, IROS 2021, https://youtu.be/L_QI9P2-ybY

Robot collisions - detection, ..., reaction

- Guess the meaning of individual blocks.

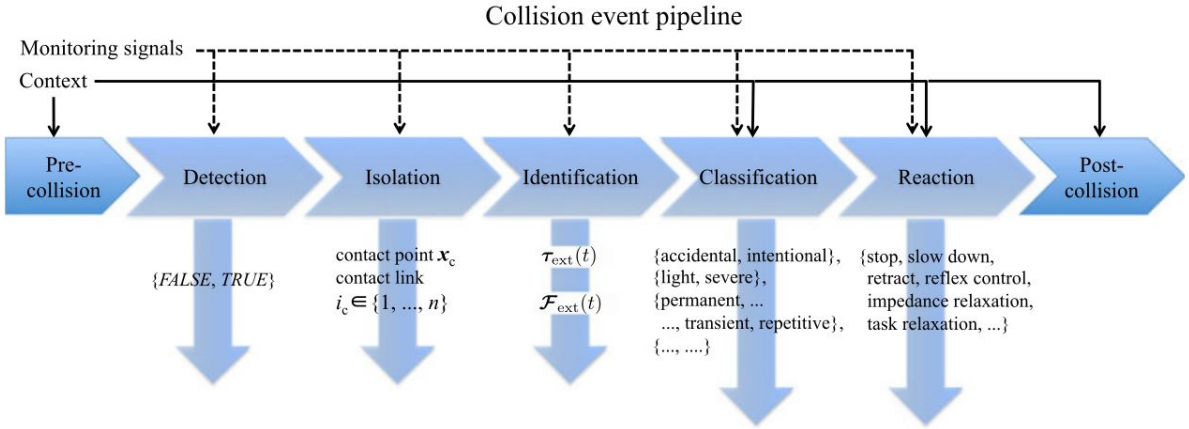

Haddadin, S., De Luca, A., & Albu-Schäffer, A. (2017). Robot collisions: A survey on detection, isolation, and identification. *IEEE Transactions on Robotics*, *33*(6), 1292-1312.

Monitoring signals

- measured currents in electrical drives
  - looking for transients possibly caused by a collision
  - comparing expected (model-based) with actual
- motor torques
  - comparing expected (model-based) with actual
- sensitive skins

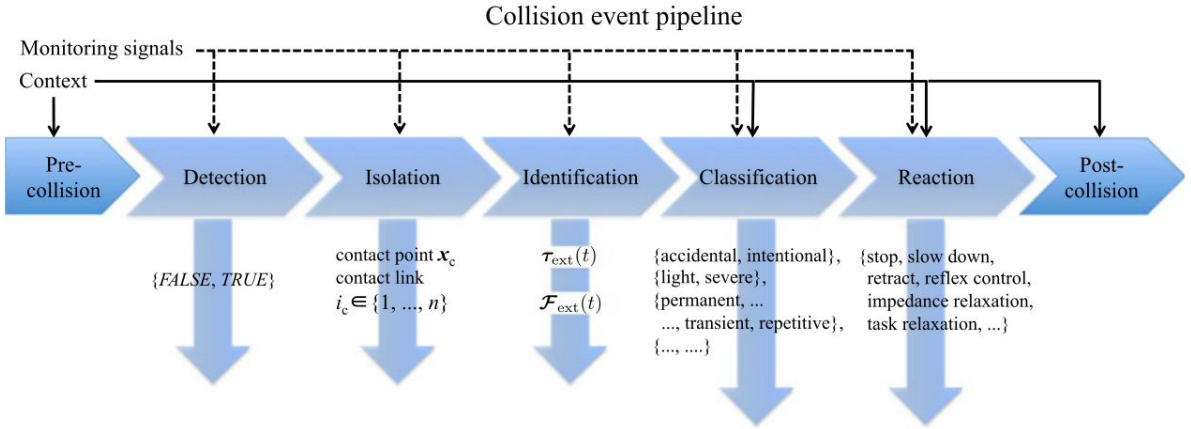

Typical assumption: there is at most a single link involved in a collision.

Haddadin, S., De Luca, A., & Albu-Schäffer, A. (2017). Robot collisions: A survey on detection, isolation, and identification. *IEEE Transactions on Robotics*, *33*(6), 1292-1312.

Collision detection

- All monitoring signals or their combination can be used…
- Relatively straightforward (at least compared to the following steps in the pipeline).

Further reading: Experimental study on UR10e: Mamedov, S., & Mikhel, S. (2020). Practical aspects of model-based collision detection. *Frontiers in Robotics and AI*, 162. https://www.frontiersin.org/articles/10.3389/frobt.2020.571574/full

Collision detection in industrial robots

- advanced option available for some robots (ABB, KUKA, UR …)
- mainly intended for detection only, not for isolation
  - based on large variations of control torques (or motor currents)

    $\|\tau(t_k) - \tau(t_{k-1})\| \geq \varepsilon \quad \Leftrightarrow \quad |\tau_i(t_k) - \tau_i(t_{k-1})| \geq \varepsilon_i$, for at least one joint i
  - based on comparison with nominal torque on the desired trajectory

    $\tau_d = M(q_d)\ddot{q}_d + S(q_d, \dot{q}_d)\dot{q}_d + g(q_d) + f(q_d, \dot{q}_d) \quad \Rightarrow \quad \|\tau - \tau_d\| \geq \varepsilon$
  - based on robot state and numerical estimate of its acceleration

    $\ddot{q}_N = \frac{d\dot{q}}{dt} \quad \Rightarrow \tau_N = M(q)\ddot{q}_N + S(q, \dot{q})\dot{q} + g(q) + f(q, \dot{q}) \quad \Rightarrow \|\tau - \tau_N\| \geq \varepsilon$
  - based on the parallel simulation of robot dynamics

    $\ddot{q}_C = M^{-1}(q)[\tau - S(q, \dot{q})\dot{q} - g(q) - f(q, \dot{q})] \quad \Rightarrow \quad \|\dot{q} - \dot{q}_C\| \geq \varepsilon_{\dot{q}}, \|q - q_C\| \geq \varepsilon_q$
- sensitive to the actual control law and reference trajectory
- require noisy acceleration estimates or on-line inversion of the robot inertia matrix

Slide from Alessandro de Luca: Physical HRI. http://www.diag.uniroma1.it/deluca/pHRI_elective/pHRI_CollisionDetectionReaction.pdf

Collision isolation

- Sensitive skin makes it easy.
- Otherwise, it is tricky.

Collision isolation and identification - relevant quantities

Robot dynamics when collision occurs:

$$M(q)\ddot{q} + C(q,\dot{q})\dot{q} + g(q) + \tau_F = \tau_m + \tau_{\text{ext}} = \tau_{\text{tot}} \quad (5)$$

where $\tau_{\text{ext}} \in \mathbb{R}^n$ is the external joint torque given by

$$\tau_{\text{ext}} = J_c^T(q)\,\mathcal{F}_{\text{ext}}. \quad (6)$$

The two active (nonconservative) terms on the right-hand side of (5) have been collectively denoted as $\tau_{\text{tot}} \in \mathbb{R}^n$, while we moved the dissipative term τ_F to the left-hand side.

The *total energy* E of the robot is the sum of its kinetic energy T and potential energy U_g due to gravity

$$E = T + U_g = \frac{1}{2}\dot{q}^T M(q)\dot{q} + U_g(q) \quad (7)$$

with $g(q) = (\partial U_g(q)/\partial q)^T$. From (5) and the skew-symmetry of $\dot{M} - 2C$, it follows that

$$\dot{E} = \dot{q}^T \tau_{\text{tot}} - \dot{q}^T \tau_F \quad (8)$$

which represents the power balance in the system, including the external power $P_{\text{ext}} = \dot{q}^T \tau_{\text{ext}}$.

The *generalized momentum* p of the robot is defined as

$$p = M(q)\dot{q}. \quad (9)$$

From (5), the time evolution of p can be written as

$$\dot{p} = \tau_{\text{tot}} - \tau_F + \dot{M}(q)\dot{q} - C(q,\dot{q})\dot{q} - g(q) \quad (10)$$

$$= \tau_{\text{tot}} - \tau_F + C^T(q,\dot{q})\dot{q} - g(q), \quad (11)$$

where (2) has been used. In particular, the ith component of $\dot{p}$ can also be written as

$$\dot{p}_i = \tau_{\text{tot},i} - \tau_{F,i} - \frac{1}{2}\dot{q}^T \frac{\partial M(q)}{\partial q_i}\dot{q} - g_i(q) \quad (12)$$

for $i = 1, \ldots, n$. Thus, each component of the generalized momentum is affected only by the associated component of the nonconservative (active and dissipative) torques. This decoupling property will be further exploited later.

Haddadin, S., De Luca, A., & Albu-Schäffer, A. (2017). Robot collisions: A survey on detection, isolation, and identification. *IEEE Transactions on Robotics*, *33*(6), 1292-1312.

Collision identification

$$M(q)\ddot{q} + C(q,\dot{q})\dot{q} + g(q) = \tau + \tau_{ext}$$

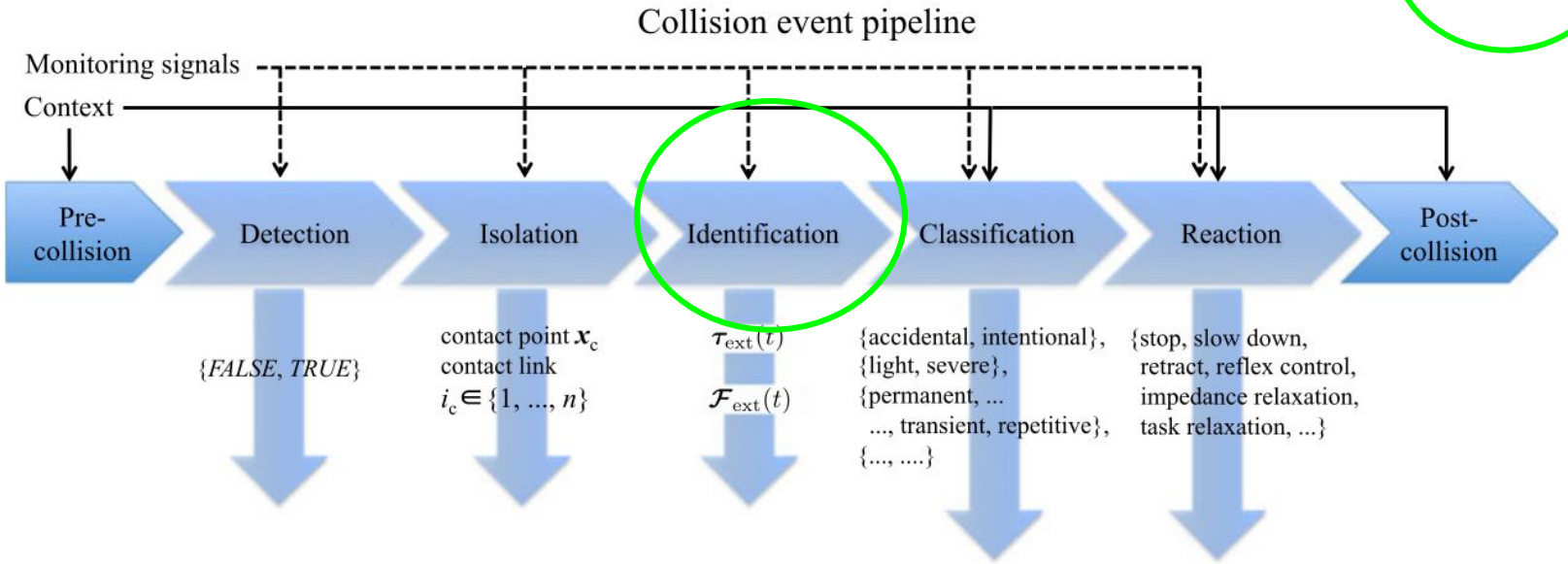

Haddadin, S., De Luca, A., & Albu-Schäffer, A. (2017). Robot collisions: A survey on detection, isolation, and identification. *IEEE Transactions on Robotics*, *33*(6), 1292-1312.

Collision detection, isolation, identification – enablers

UR10 motor current sensors only

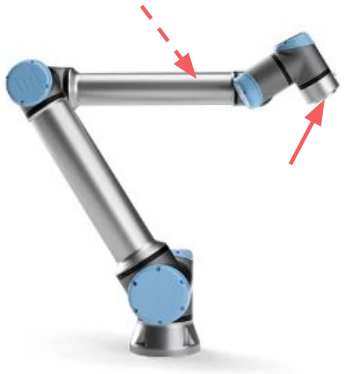

UR10e motor current sensors + wrist F/T sensor

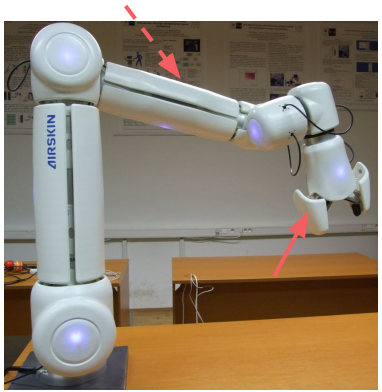

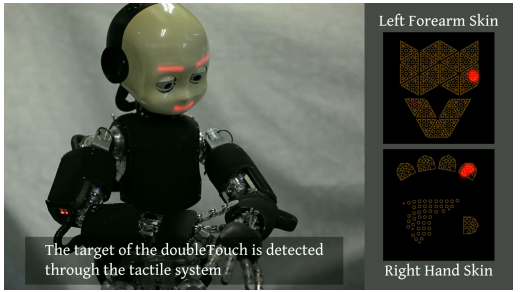

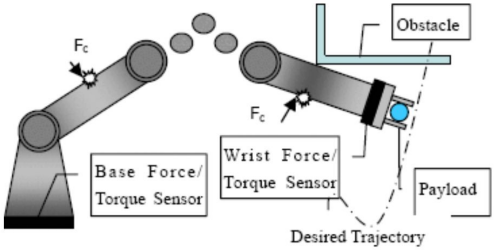

Lu, S., Chung, J. H., & Velinsky, S. A. (2005, April). Human-robot collision detection and identification based on wrist and base force/torque sensors. In *Proceedings of the 2005 IEEE international Conference on Robotics and Automation* (pp. 3796-3801). IEEE.

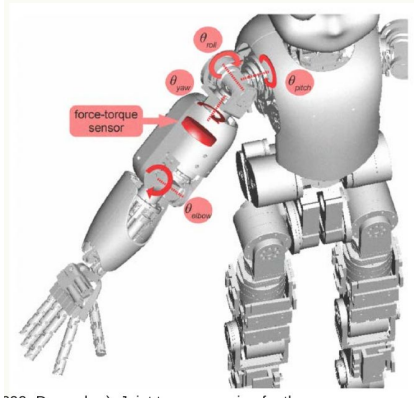

Collision detection, isolation, identification - enablers (2)

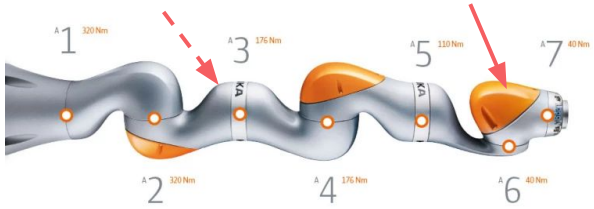

KUKA LBR iiwa
joint torque sensors
in every axis

https://www.wevolver.com/wevolver.staff/kuka.lbr.iiwa

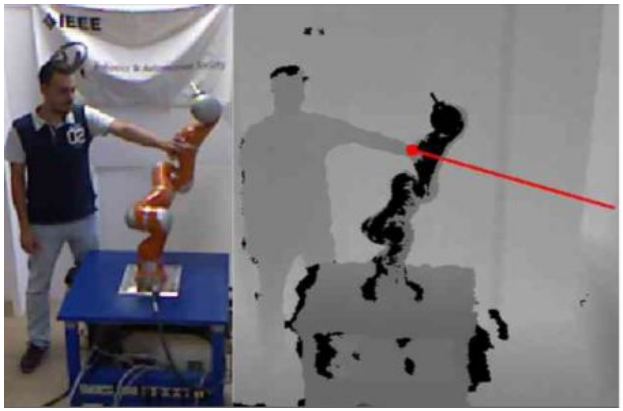

http://www.diag.uniroma1.it/deluca/pHRI_elective/pHRI_CoexistenceCollaboration.pdf

Direct estimation of τ_{ext}

joint torque sensors

$$\tau = M(q)\ddot{q} + C(q,\dot{q})\dot{q} + g(q) + \tau_F + \tau_{ext} = \tau_{dyn} + \tau_{ext}$$

$M(q) \in \mathbb{R}^{n\times n}$ joint space inertia matrix

$C(q,\dot{q})\dot{q} \in \mathbb{R}^n$ centripedal and Coriolis vector

$g(q) \in \mathbb{R}^n$ gravity vector

$\tau \in \mathbb{R}^n$ joint torque measured by sensor

$\tau_{dyn} \in \mathbb{R}^n$ torque computed from dynamics

- results from the configuration, velocity and acceleration of the robot
- can be obtained with dynamics simulator (e.g. OpenRave)

$\tau_F \in \mathbb{R}^n$ dissipative friction torque

$\tau_{ext} \in \mathbb{R}^n$ external joint torque $(\tau_{ext} = J^T(q)\mathcal{F}_{ext})$

$$\tau_{ext} = \tau - \tau_{dyn}$$

B. Direct Estimation of τ_{ext}

Using (5), the algebraic estimation of the external joint torque τ_{ext} is

$$\hat{\tau}_{ext} = \hat{M}(q)\ddot{q} + \hat{C}(q,\dot{q})\dot{q} + \hat{g}(q) - \tau_m . \qquad (31)$$

This is indeed the most direct monitoring method, which uses the motor torque and the link position, velocity, and acceleration. Unfortunately, this approach is not applicable in practice, since typically only q is measured and its double differentiation (to be performed on line) leads to the inclusion of nonnegligible noise in the estimation process. One might think of introducing acceleration sensors at the joints or on the links [56], but this increases system complexity significantly.

Haddadin, S., De Luca, A., & Albu-Schäffer, A. (2017). Robot collisions: A survey on detection, isolation, and identification. *IEEE Transactions on Robotics*, *33*(6), 1292-1312.

Other ways of estimating $\boldsymbol{\tau}_{ext}$

A. Estimation of the power P_{ext} associated with the external joint torque via energy observer.
B. [Direct estimation of $\boldsymbol{\tau}_{ext}$.]
C. Monitoring $\boldsymbol{\tau}_{ext}$ via inverse dynamics.
D. Estimation of $\boldsymbol{\tau}_{ext}$ via joint velocity observer.
E. Estimation of $\boldsymbol{\tau}_{ext}$ via momentum observer.

For details and equations see: Haddadin, S., De Luca, A., & Albu-Schäffer, A. (2017). Robot collisions: A survey on detection, isolation, and identification. *IEEE Transactions on Robotics*, *33*(6), 1292-1312.

TABLE I
COLLISION MONITORING METHODS FOR RIGID ROBOTS

	Monitoring method	Computational effort	Measurement quantities	Advantages	Disadvantages
Absolute motor torque	$\lvert\boldsymbol{\tau}_m\rvert \geq \boldsymbol{\tau}_{m,\max}$	complexity : $*$ memory : $*$ dual use : no **overall** : $*$	$\boldsymbol{\tau}_m = \boldsymbol{K}_i \boldsymbol{i}_m$	– extremely simple – needs only $\boldsymbol{i}_m$	– heuristic – friction dependent – low sensitivity – no isolation/identification
Motor torque change	$\lvert\dot{\boldsymbol{\tau}}_m\rvert \geq \dot{\boldsymbol{\tau}}_{m,\max}$	complexity : $*$ memory : $*$ dual use : no **overall** : $*$	$\boldsymbol{\tau}_m = \boldsymbol{K}_i \boldsymbol{i}_m$ $\dot{\boldsymbol{\tau}}_m = \boldsymbol{K}_i \dot{\boldsymbol{i}}_m$	– extremely simple – needs only $\boldsymbol{i}_m$	– heuristic – friction dependent – low sensitivity – $\dot{\boldsymbol{i}}_m$ required – no isolation/identification
Motor torque tube	$\hat{\boldsymbol{\tau}}_{\text{ext}} \approx$ $\boldsymbol{\tau}_{m,\text{ref}} - \boldsymbol{\tau}_m$	complexity : $*$ memory : $****$ dual use : no **overall** : $*$	$\boldsymbol{\tau}_m = \boldsymbol{K}_i \boldsymbol{i}_m$	– simple – model free – friction independent	– controller/trajectory dependent – only suitable for accurate tracking – needs prior execution – large data storage

Haddadin, S., De Luca, A., & Albu-Schäffer, A. (2017). Robot collisions: A survey on detection, isolation, and identification. *IEEE Transactions on Robotics*, *33*(6), 1292-1312.

Energy observer	Eq. (26); property: Eq. (27)	$\frac{1}{2}\dot{\boldsymbol{q}}^T \mathrm{NE}_{\mathbf{0}}(\boldsymbol{q}, \mathbf{0}, \dot{\boldsymbol{q}})$ complexity : $**$ memory : $**$ dual use : partly **overall** : $**$	$\boldsymbol{\tau}_m = \boldsymbol{K}_i \boldsymbol{i}_m$ $\boldsymbol{q}, \dot{\boldsymbol{q}}$	– simple – only $\boldsymbol{M}(\boldsymbol{q})\dot{\boldsymbol{q}}$, no inversion – some identification	– no detection if – $\dot{\boldsymbol{q}} \equiv \mathbf{0}$ – $\mathcal{F}_{\mathrm{ext}} \perp \boldsymbol{V}_c$ – no isolation
Direct estimation	Eq. (31)	$\mathrm{NE}_{\boldsymbol{g}_0}(\boldsymbol{q}, \dot{\boldsymbol{q}}, \ddot{\boldsymbol{q}})$ complexity : $*****$ memory : $*$ dual use : yes **overall** : $***$	$\boldsymbol{\tau}_m = \boldsymbol{K}_i \boldsymbol{i}_m$ $\boldsymbol{q}, \dot{\boldsymbol{q}}, \ddot{\boldsymbol{q}}$	– ideal model – moderately complex – only $\boldsymbol{M}(\boldsymbol{q})$, no inversion – isolation/identification possible	– $\ddot{\boldsymbol{q}}$ required – full dynamics necessary – friction dependent
Inverse dynamics	$\hat{\boldsymbol{\tau}}_{\mathrm{ext}} \approx \hat{\boldsymbol{\tau}}_{m,\mathrm{ff}} - \boldsymbol{\tau}_m$; $\hat{\boldsymbol{\tau}}_{m,\mathrm{ff}}$ from Eq. (33)	$\mathrm{NE}_{\boldsymbol{g}_0}(\boldsymbol{q}_\mathrm{d}, \dot{\boldsymbol{q}}_\mathrm{d}, \ddot{\boldsymbol{q}}_\mathrm{d})$ complexity : $*****$ memory : $**$ dual use : no **overall** : $*****$	$\boldsymbol{\tau}_m = \boldsymbol{K}_i \boldsymbol{i}_m$	– no position sensor dependency – isolation/identification possible – feedforward computed anyway	– controller/trajectory dependent – calculate dynamics twice

Haddadin, S., De Luca, A., & Albu-Schäffer, A. (2017). Robot collisions: A survey on detection, isolation, and identification. *IEEE Transactions on Robotics*, *33*(6), 1292-1312.

Velocity observer	Eq. (38); property: Eq. (41)	$\mathrm{NE}_{\boldsymbol{g}_0}(\boldsymbol{q}, \dot{\boldsymbol{q}}, \boldsymbol{0})$ $n \times \mathrm{NE}_{\boldsymbol{0}}(\boldsymbol{q}, \dot{\boldsymbol{q}}, \boldsymbol{e}_i)$ $\hat{\boldsymbol{M}}^{-1}$ complexity : $*****$ memory : $*$ dual use : partly **overall** : $*$	$\boldsymbol{\tau}_m = \boldsymbol{K}_i \boldsymbol{i}_m$ $\boldsymbol{q}, \dot{\boldsymbol{q}}$	– $\ddot{\boldsymbol{q}}$ not needed – isolation/identification possible – further use for state recovery	– sensitivity depends on $\boldsymbol{q}$ – full dynamics required
Momentum observer	Eq. (46); property: Eq. (47)	$\mathrm{NE}_{\boldsymbol{g}_0}(\boldsymbol{q}, \dot{\boldsymbol{q}}, \boldsymbol{0})$ $n \times \mathrm{NE}_{\boldsymbol{0}}(\boldsymbol{q}, \boldsymbol{0}, \dot{\boldsymbol{q}}_i \boldsymbol{e}_i / T_s)$ $\mathrm{NE}_{\boldsymbol{0}}(\boldsymbol{q}, \boldsymbol{0}, \dot{\boldsymbol{q}})$ OR customized dynamics OR $\mathrm{NE}_{\boldsymbol{g}_0}(\boldsymbol{q}, \dot{\boldsymbol{q}}, \boldsymbol{0})$ $n \times \mathrm{MNE}_{\boldsymbol{0}}(\boldsymbol{q}, \dot{\boldsymbol{q}}, \boldsymbol{e}_i, \boldsymbol{0})$ $\mathrm{NE}_{\boldsymbol{0}}(\boldsymbol{q}, \boldsymbol{0}, \dot{\boldsymbol{q}})$ complexity : $*****$ memory : $*$ dual use : partly **overall** : $****$	$\boldsymbol{\tau}_m = \boldsymbol{K}_i \boldsymbol{i}_m$ $\boldsymbol{q}, \dot{\boldsymbol{q}}$	– $\ddot{\boldsymbol{q}}$ not needed – isolation possible – only $\boldsymbol{M}(\boldsymbol{q})$, no inversion – sensitivity independent of $\boldsymbol{q}$	– full dynamics necessary – $\dot{\boldsymbol{M}}(\boldsymbol{q})$ required – (or n calls of modified NE for $\boldsymbol{C}^T(\boldsymbol{q}, \dot{\boldsymbol{q}})$)

Haddadin, S., De Luca, A., & Albu-Schäffer, A. (2017). Robot collisions: A survey on detection, isolation, and identification. *IEEE Transactions on Robotics*, *33*(6), 1292-1312.

Robot reaction to collision

- Stop
  - Pros:
    - simple, few requirements (collision detection is enough)
  - Cons:
    - may possibly lead to inconvenient situations, where the robot is unnaturally constraining or blocking the human
- Torque control with gravity compensation
  - robot moves along a desired trajectory with a position reference-based controller (e.g., position or impedance control).
  - after detection, the control mode is switched to a compliance-based controller that ignores the previous task trajectory. A particularly useful variant is to switch to torque control mode with gravity compensation. Note that this strategy does not explicitly take into account any information about $\boldsymbol{\tau}_{ext}$.

Haddadin, S., & Croft, E. (2016). Physical human–robot interaction. In *Springer Handbook of Robotics* (pp. 1835-1874). Springer, Cham.

Gravity compensation

https://youtu.be/1Or0kym2uic

Robot reaction strategies

- upon detection of a collision (r is over some threshold)
  - no reaction (strategy 0): robot continues its planned motion…
  - stop robot motion (strategy 1): either by braking or by stopping the motion reference generator and switching to a high-gain position control law
  - reflex* strategy: switch to a residual-based control law

$$\tau' = K_R r \qquad K_R > 0 \quad \text{(diagonal)}$$

"joint torque command in same direction of collision torque"

* = in robots with transmission/joint elasticity, the reflex strategy can be implemented in different ways (strategies 2, 3, 4)

- strategy 2 floating reaction (robot ≈ in "zero-gravity")

$$\tau_{J,d} = \bar{g}(\theta) \qquad K_P = 0$$

- strategy 3 reflex torque reaction (closest to the rigid case)

$$\tau_{J,d} = K_R r_{\mathrm{EJ}} + \bar{g}(\theta) \qquad K_P = 0$$

- strategy 4 admittance mode reaction (residual r_{EJ} is used as the new reference for the motor velocity)

$$\tau_{J,d} = \bar{g}(\theta) \qquad \dot{\theta}_d = K_{R,\theta}\, r_{\mathrm{EJ}}$$

Slides from Alessandro de Luca: Physical HRI. http://www.diag.uniroma1.it/deluca/pHRI_elective/pHRI_CollisionDetectionReaction.pdf

Reaction to collision - videos 1

stop (strategy 0)

gravity compensation (strategy 2)

Slide from Alessandro de Luca: Physical HRI. http://www.diag.uniroma1.it/deluca/pHRI_elective/pHRI_CollisionDetectionReaction.pdf

Robot reaction to collision

- Stop
- Torque control with gravity compensation
- Torque reflex
  - needs $\boldsymbol{\tau}_{\text{ext}}$
- Admittance reflex
  - needs $\boldsymbol{\tau}_{\text{ext}}$
- Move away
  - needs $\boldsymbol{F}_{\text{ext}}$

Torque Reflex. This strategy extends the torque control-based strategy by explicitly incorporating the estimation or measurement of $\boldsymbol{\tau}_{\text{ext}}$ into the motor torque $\boldsymbol{\tau}$ via

$$\boldsymbol{\tau} = \hat{\boldsymbol{g}}(\boldsymbol{q}) + (\mathbf{I} - \mathbf{K}_{\text{r}})\boldsymbol{\tau}_{\text{ext}}\,, \tag{69.26}$$

where $\mathbf{K}_{\text{r}} = \text{diag}\{k_{\text{r},i}\} > 1$. It can be shown that, under sufficiently accurate estimates or measurements, such a law is equivalent to scaling of the robot dynamics by $\mathbf{K}_r^{-1}$. The closed-loop dynamics become

$$\underbrace{\mathbf{K}_r^{-1}\mathbf{M}(\boldsymbol{q})}_{\mathbf{M}'(\boldsymbol{q})}\ddot{\boldsymbol{q}} + \mathbf{K}_r^{-1}\mathbf{C}(\boldsymbol{q},\dot{\boldsymbol{q}})\dot{\boldsymbol{q}} + \boldsymbol{\tau}_{\text{ext}} = \mathbf{0}\,, \tag{69.27}$$

where $\mathbf{M}(\boldsymbol{q}) > \mathbf{M}'(\boldsymbol{q})$ holds component-wise.

Admittance Reflex. Reference trajectory modification via an admittance-type strategy that uses the measurement or estimation of $\boldsymbol{\tau}_{\text{ext}}$ can easily, for example, be realized via

$$\boldsymbol{q}_{\text{d}}(t) = -\int_{t_{\text{c}}}^{\text{T}} \mathbf{K}_{\text{a}}\boldsymbol{\tau}_{\text{ext}}\,\text{d}t\,, \tag{69.28}$$

where $\mathbf{K}_{\text{a}} = \text{diag}\{k_{\text{a},i}\} > 1$. With this scheme that requires no control switching the robot quickly drives away from the external torque source and decreases the contact forces till they decay to zero.

Haddadin, S., & Croft, E. (2016). Physical human–robot interaction. In *Springer Handbook of Robotics* (pp. 1835-1874). Springer, Cham.

Reaction to collision – videos 2

admittance mode (strategy 4)

reflex torque (strategy 3)

Slide from Alessandro de Luca: Physical HRI. http://www.diag.uniroma1.it/deluca/pHRI_elective/pHRI_CollisionDetectionReaction.pdf

Experimental comparison of strategies
balloon impact

- residual and velocity at joint 4 with various reaction strategies

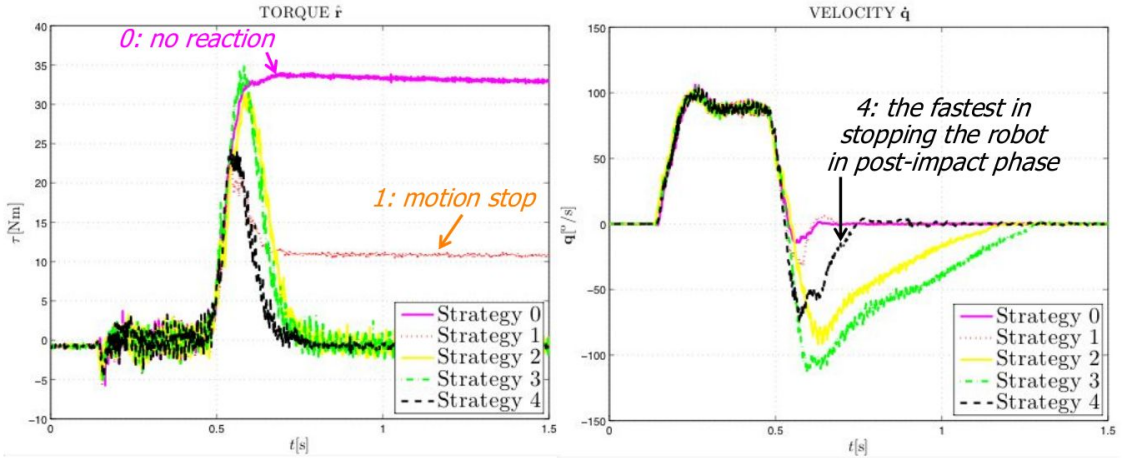

impact at 90°/sec with coordinated joint motion

Slide from Alessandro de Luca: Physical HRI. http://www.diag.uniroma1.it/deluca/pHRI_elective/pHRI_CollisionDetectionReaction.pdf

Combining power and force limiting (PFL) with speed and separation monitoring (SSM)

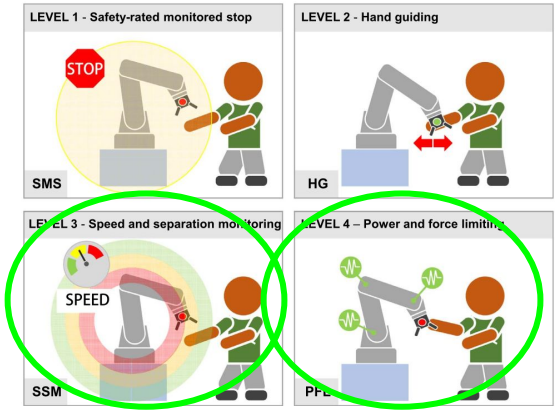

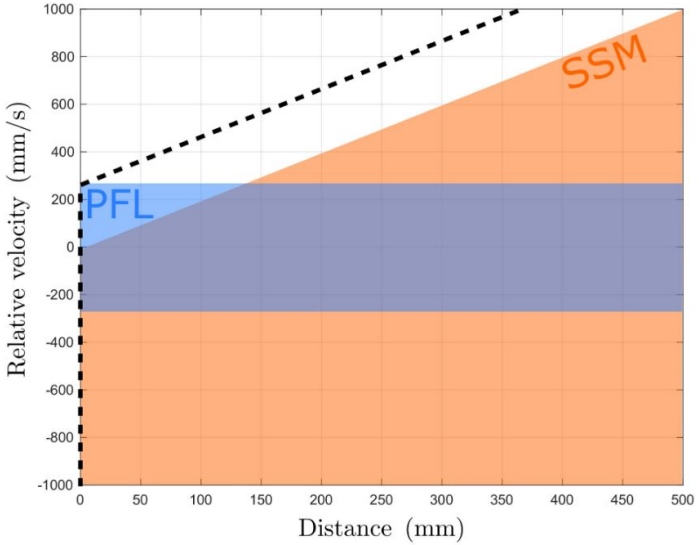

Lucci, N., Lacevic, B., Zanchettin, A. M., & Rocco, P. (2020). Combining speed and separation monitoring with power and force limiting for safe collaborative robotics applications. *IEEE Robotics and Automation Letters*, *5*(4), 6121-6128.

SSM & PFL

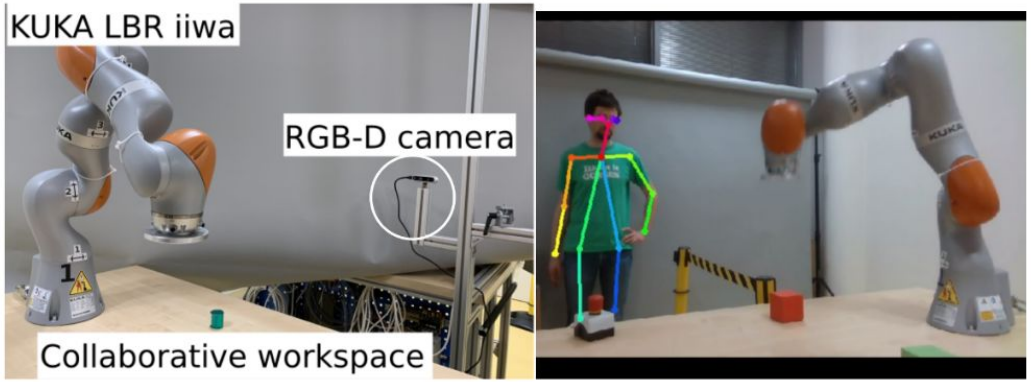

	Stop full Nose	from speed Wrist	Reduce	speed	Stop reduced Nose	from speed Wrist
			Nose	Wrist		
End-effector	1.28	1.33	1.44	1.49	0.71	0.76
3	1.33	1.38	1.49	1.54	0.76	0.81
Base	1.28	1.33	1.44	1.49	0.71	0.76

TABLE II: Effective keypoint-pair protective separation distance in meters.

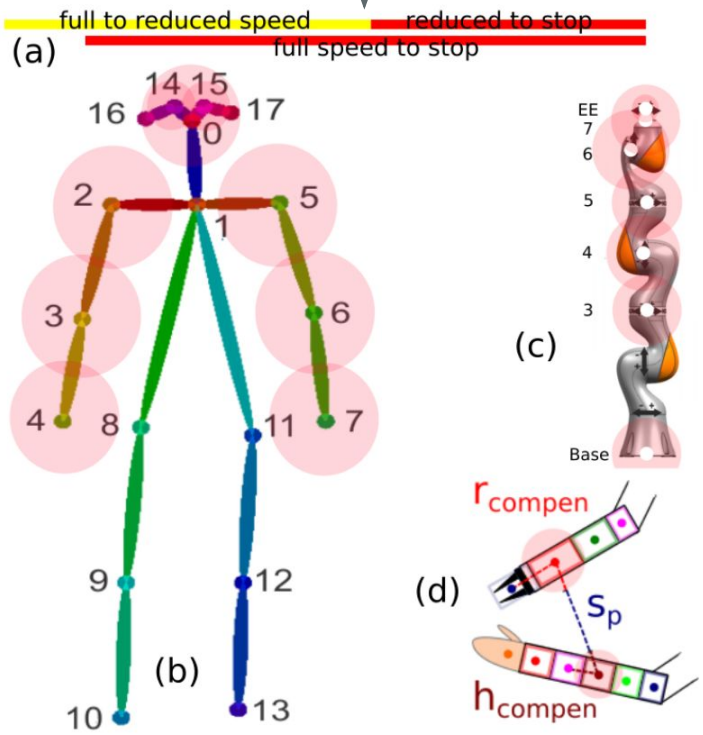

Recall separation distance from ISO/TS 15066:

$$S_p(t_0) = S_\mathrm{h} + S_\mathrm{r} + S_\mathrm{s} + C + Z_\mathrm{d} + Z_\mathrm{r}$$

Svarny, P., Tesar, M., Behrens, J. K., & Hoffmann, M. (2019, November). Safe physical HRI: Toward a unified treatment of speed and separation monitoring together with power and force limiting. In *2019 IEEE/RSJ International Conference on Intelligent Robots and Systems (IROS)* (pp. 7580-7587). IEEE.

SSM & PFL

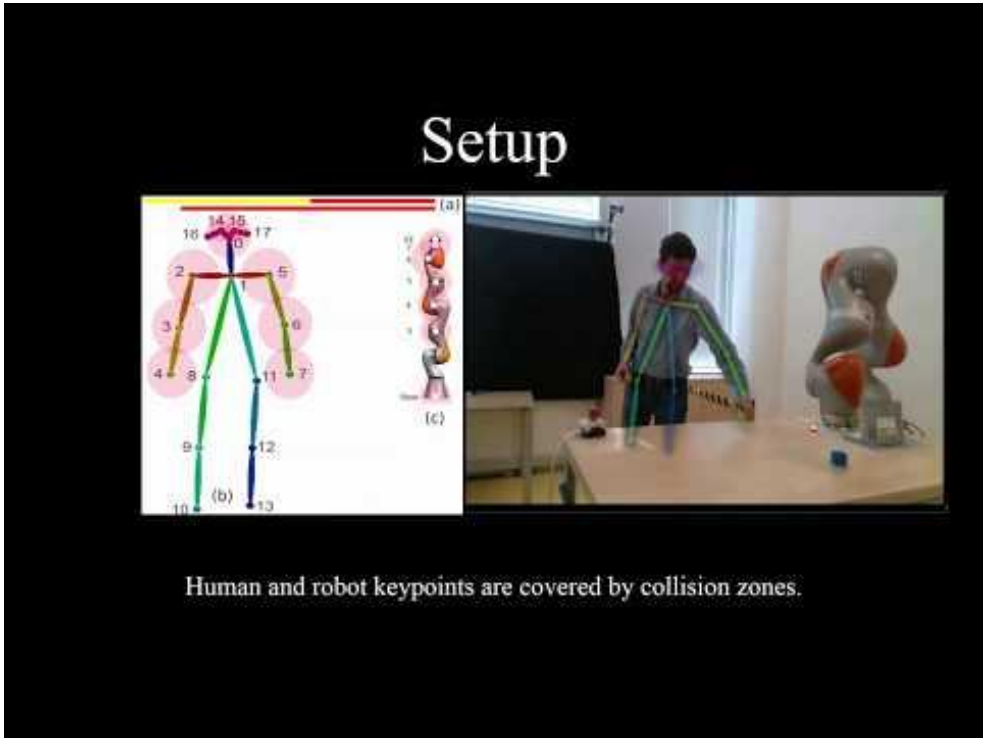

Svarny, P., Tesar, M., Behrens, J. K., & Hoffmann, M. (2019, November). Safe physical HRI: Toward a unified treatment of speed and separation monitoring together with power and force limiting. In *2019 IEEE/RSJ International Conference on Intelligent Robots and Systems (IROS)* (pp. 7580-7587). IEEE.

H. Power and force limiting

The SSM regime prescribes that the robot stops before contact occurs. In our approach, we also allow the robot to slow down so that it can operate in the PFL regime, see below. We assume the end-effector exerts pressure on a surface area of at least 1 cm ^{2}.

We can calculate the maximal relative speed of the system for a transient contact given the surface and the robot weight. For this, we use the formula A.6 from [2]. This equation also asks for some preliminary calculations, like for example μ, the reduced mass for the two body system of the robot and the human operator. We summarize the calculation here. In order to ascertain absolute safety, we assume the worst case scenario, i.e. an impact in the chest. The values for m_{h}, $p_{\max}$ and k are taken from the appropriate tables in [2].

$$m_{\mathrm{r}} = \frac{M}{2} + m_L = \frac{23.9}{2} + 0 \tag{8}$$

$$\mu = \left(\frac{1}{m_{\mathrm{h}}} + \frac{1}{m_{\mathrm{r}}}\right)^{-1} = \left(\frac{1}{40} + \frac{2}{23.9}\right)^{-1} \tag{9}$$

$$v_{rel,max} = \frac{p_{max} \cdot A}{\sqrt{\mu \cdot K}} = \frac{2.4 \times 10^6 \cdot 1 \times 10^{-4}}{\sqrt{\mu \cdot 2.5 \times 10^4}} = 0.50 \tag{10}$$

Thus we know that the speed of 0.42 m/s is a conservative speed in order to be in the PFL regime. We determine the distance at which the robot needs to start slowing down to be PFL compliant in the same way as we did with SSM in Eq. 7. However, we take into account only the difference between 1 m/s and 0.42 m/s. The resulting value for S_p is 0.73 m (full to reduced speed). The stopping distance for 0.42 m/s according to the equation would be 0.60 m (reduced to stop). According to [2], non-zero energy contact with the human head is not allowed. Thus our final setup forces the robot to stop on the proximity of the human head (see Section IV-C).

Why is the SSM & PFL fastest?

1. Higher speed - needs to break to reduced speed only.
2. Task continues in reduced speed even when operator is around.

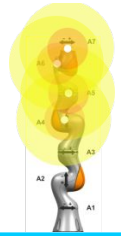
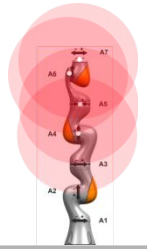
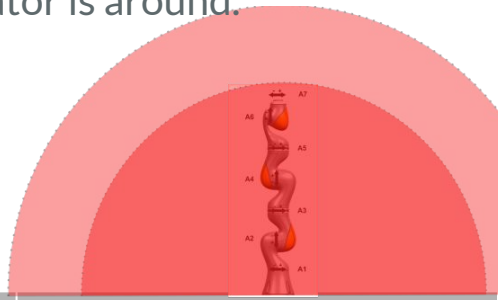

Our	PFL	SSM	Stop zone
228 s	256 s	257 s	267 s

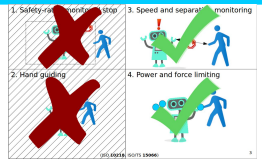
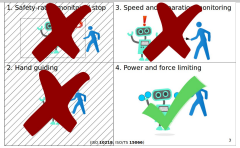
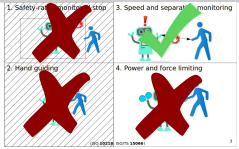
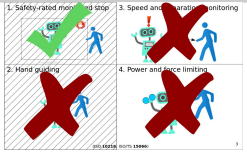

Reference (full speed): 154 s

Svarny, P., Tesar, M., Behrens, J. K., & Hoffmann, M. (2019, November). Safe physical HRI: Toward a unified treatment of speed and separation monitoring together with power and force limiting. In *2019 IEEE/RSJ International Conference on Intelligent Robots and Systems (IROS)* (pp. 7580-7587). IEEE.

Collaborative robot regimes

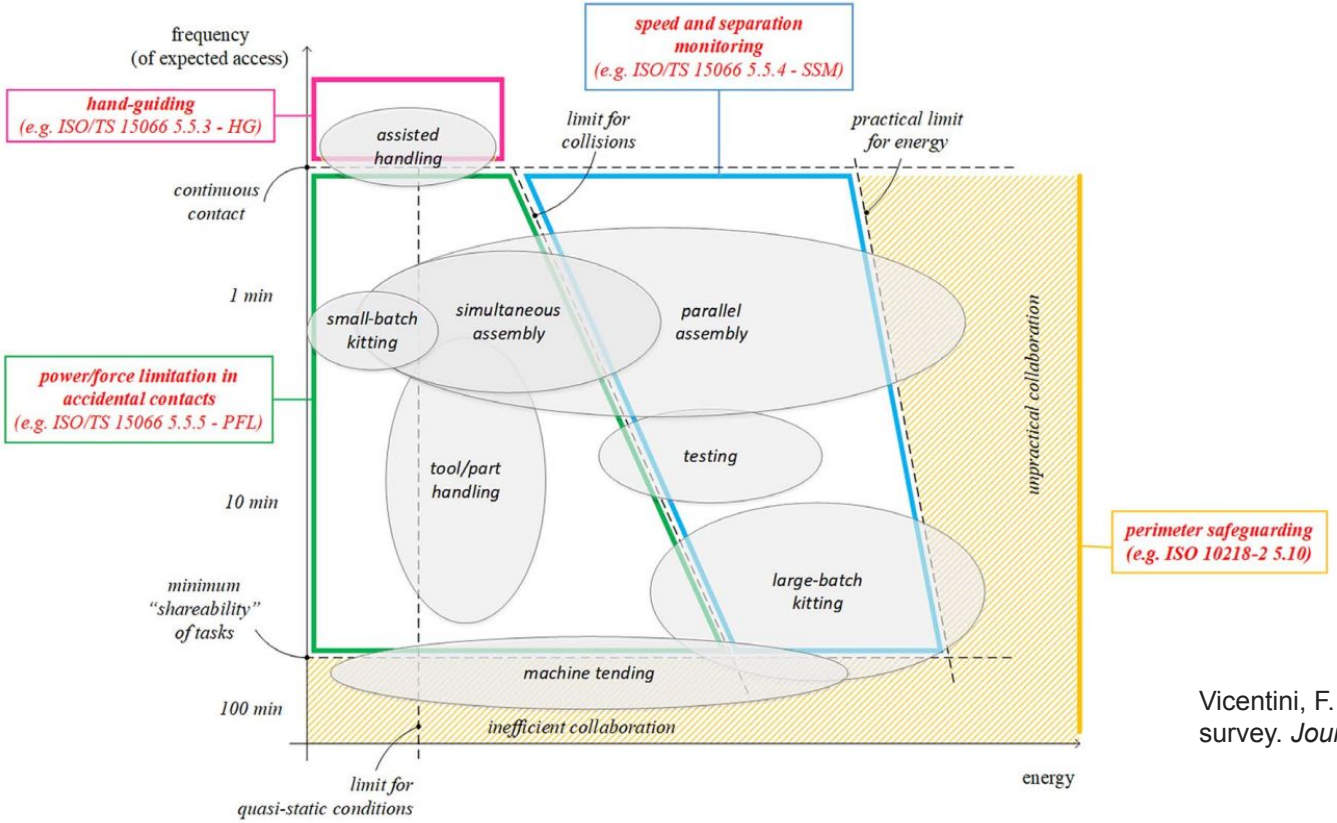

Vicentini, F. (2021). Collaborative robotics: a survey. *Journal of Mechanical Design*, *143*(4).

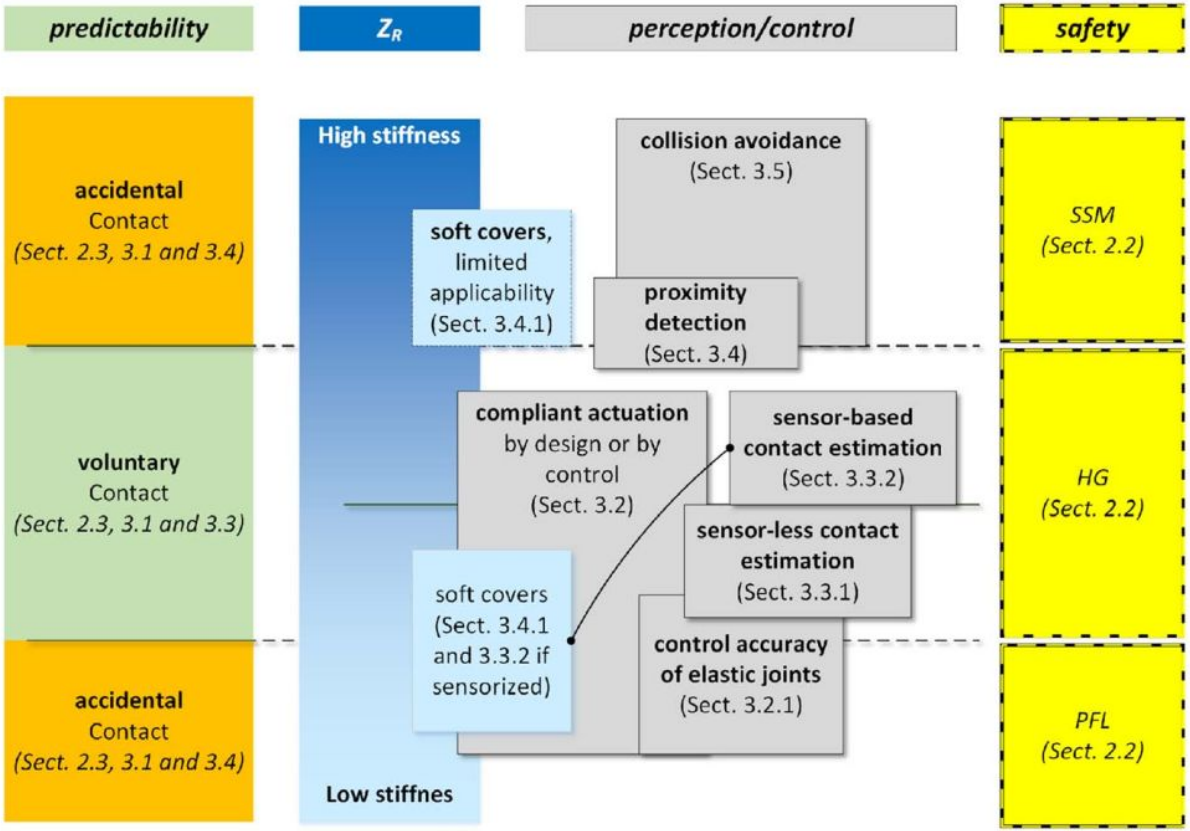

Vicentini, F. (2021). Collaborative robotics: a survey. *Journal of Mechanical Design*, *143*(4).

Resources and further reading

- Books / book sections
  - Haddadin, S., & Croft, E. (2016). Physical human–robot interaction. In *Springer Handbook of Robotics* (pp. 1835-1874). Springer, Cham.
  - 8.1.3 “Understanding the mass matrix” in Lynch, K. M., & Park, F. C. (2017). Modern robotics. Cambridge University Press.
- Online resources
  - https://sites.google.com/site/matejhof/research/cobots-and-hri
  - video lectures by Kevin Lynch (covering Lynch, K. M., & Park, F. C. (2017). Modern robotics.)
    - https://modernrobotics.northwestern.edu/nu-gm-book-resource/8-1-3-understanding-the-mass-matrix
    - https://modernrobotics.northwestern.edu/nu-gm-book-resource/8-6-dynamics-in-the-task-space/
  - Federico Vicentini - presentations
    - Safety of collaborative robotics. Overview and critical issues. 2019. https://www.etui.org/sites/default/files/ez_import/2019_ETUI_vicentini_collaborative%20robotics.pdf
  - Alessandro de Luca
    - Physical HRI - Lecture slides by Alessandro de Luca: http://www.diag.uniroma1.it/deluca/pHRI.php.
    - Youtube playlist: https://www.youtube.com/playlist?list=PLvAUmIzqq6oaRtwX9l9sjDhcNMXNCGSN0
    - Talks on youtube. E.g., https://youtu.be/L_QI9P2-ybY
- Articles
  - Khatib, O. (1995). Inertial properties in robotic manipulation: An object-level framework. *The International Journal of Robotics Research*, *14*(1).
  - Haddadin, S., De Luca, A., & Albu-Schäffer, A. (2017). Robot collisions: A survey on detection, isolation, and identification. *IEEE Transactions on Robotics*, *33*(6), 1292-1312.
  - Kirschner, R. J., Mansfeld, N., Peña, G. G., Abdolshah, S., & Haddadin, S. (2021, March). Notion on the Correct Use of the Robot Effective Mass in the Safety Context and Comments on ISO/TS 15066. In *2021 IEEE International Conference on Intelligence and Safety for Robotics (ISR)* (pp. 6-9). IEEE.

Safety Tree

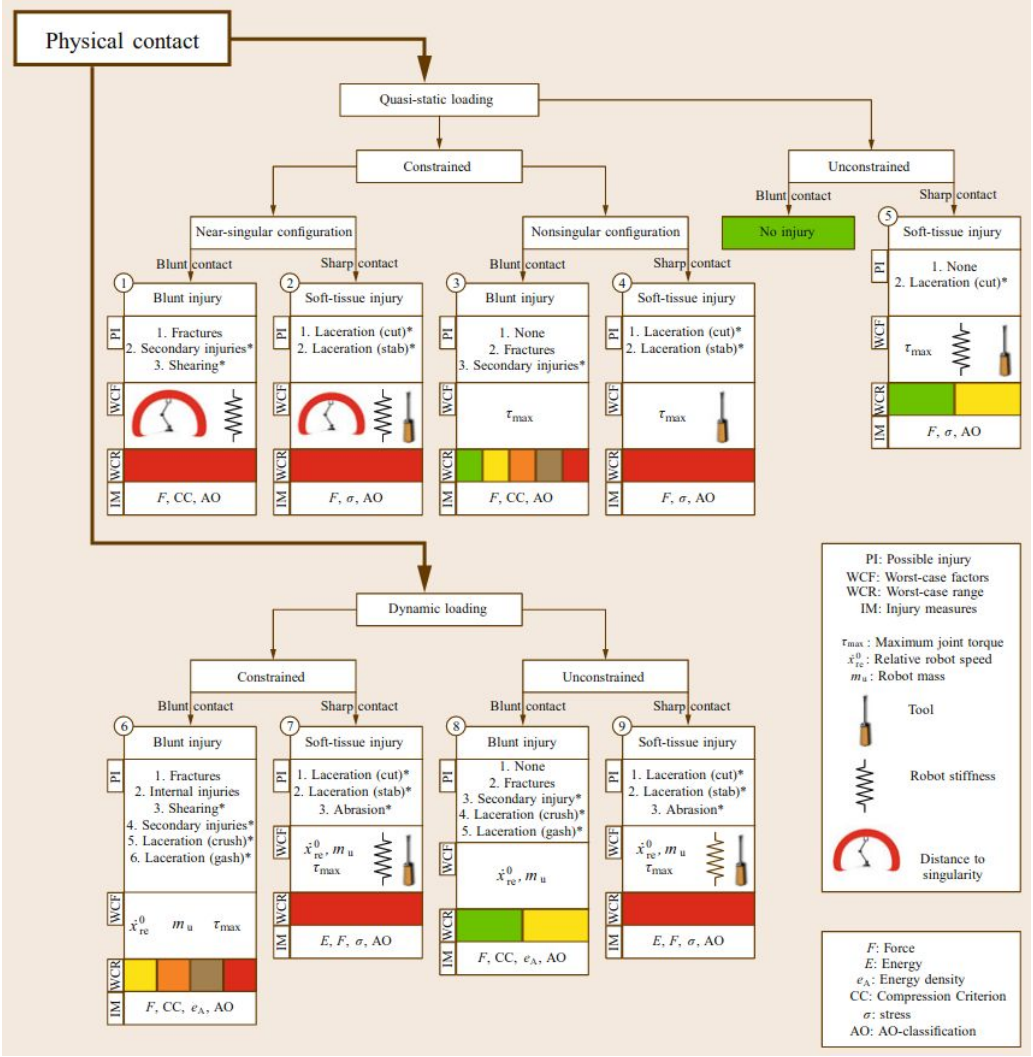

Haddadin, S., & Croft, E. (2016). Physical human–robot interaction. In *Springer handbook of robotics* (pp. 1835-1874). Springer, Cham.

Back to SSM & PFL together I

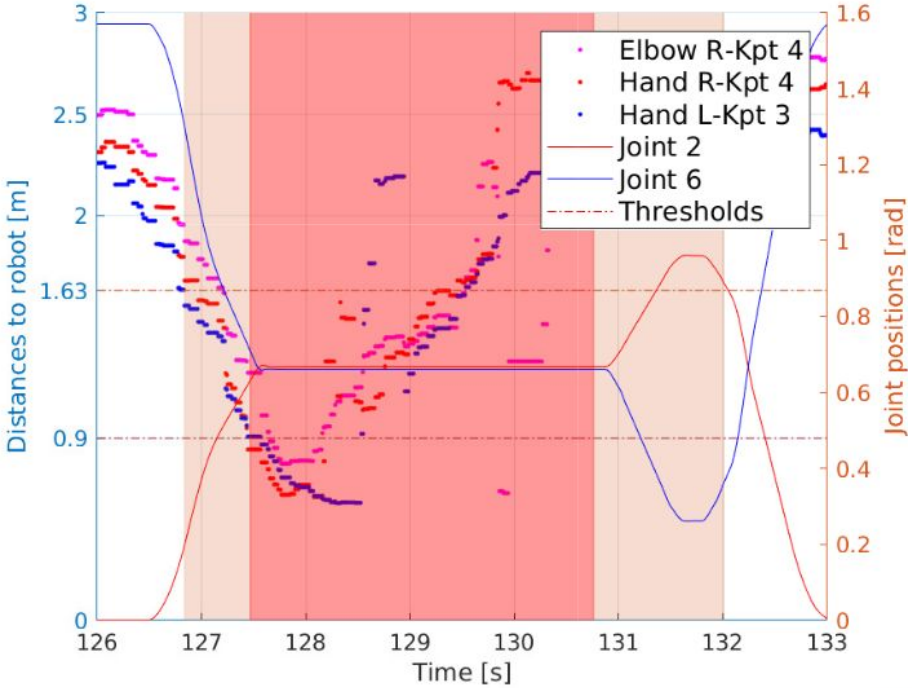

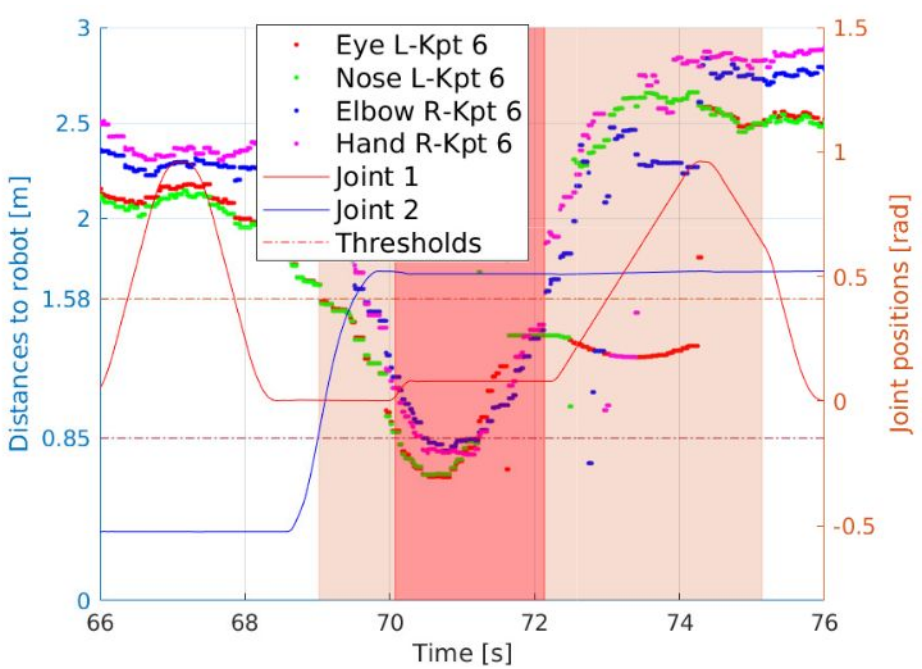

Full sp.	Reduced sp.	Sc. 1	Sc. 2	Sc. 3	Sc. 4	Sc. 5
154	256	267	254	257	231	228

TABLE III: Task duration for different scenarios in seconds.

Svarny, P., Tesar, M., Behrens, J. K., & Hoffmann, M. (2019, November). Safe physical HRI: Toward a unified treatment of speed and separation monitoring together with power and force limiting. In *2019 IEEE/RSJ International Conference on Intelligent Robots and Systems (IROS)* (pp. 7580-7587). IEEE.

Back to SSM & PFL together II - theory

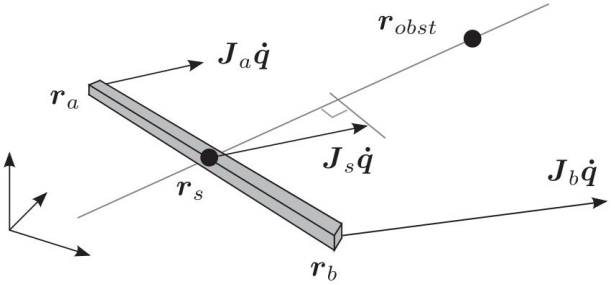

Robot link parameterization w.r.t. point

$$g(s,\dot{\boldsymbol{q}}) \equiv \dot{\boldsymbol{q}}^T\boldsymbol{\beta}(s) - \frac{\|\boldsymbol{r}_{os}\|^2}{T_s} = \alpha_2 s^2 + \alpha_1 s + \alpha_0, \qquad (11)$$

where $\alpha_2 = -\|\boldsymbol{r}_{ba}\|^2/T_s$, $\alpha_1 = a_1 + 2\boldsymbol{r}_{oa}^T/T_s\boldsymbol{r}_{ba}$, $\alpha_0 = a_0 - \|\boldsymbol{r}_{oa}\|^2/T_s$. Now, the inequality (8) becomes:

$$g(s,\dot{\boldsymbol{q}}) \leq C\sqrt{\boldsymbol{\beta}^T(s)\boldsymbol{B}^{-1}\boldsymbol{\beta}(s)}. \qquad (12)$$

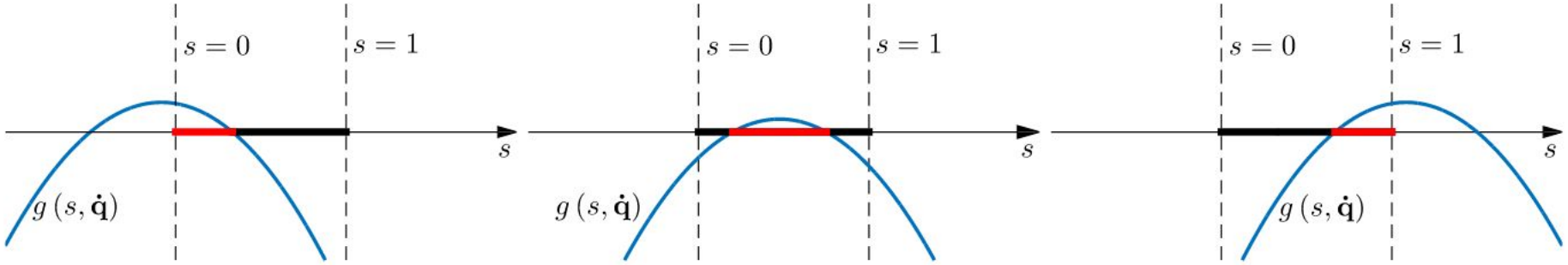

Fig. 3. Three cases that may occur when $g(s,\dot{\boldsymbol{q}})$ changes sign in $s \in [0,1]$. In each scenario, the subset where $g(s,\dot{\boldsymbol{q}}) > 0$ is connected (shown in red).

Lucci, N., Lacevic, B., Zanchettin, A. M., & Rocco, P. (2020). Combining speed and separation monitoring with power and force limiting for safe collaborative robotics applications. *IEEE Robotics and Automation Letters*, *5*(4), 6121-6128.

Back to SSM & PFL together II - setup

Lucci, N., Lacevic, B., Zanchettin, A. M., & Rocco, P. (2020). Combining speed and separation monitoring with power and force limiting for safe collaborative robotics applications. *IEEE Robotics and Automation Letters*, *5*(4), 6121-6128.

Back to SSM & PFL together II - results

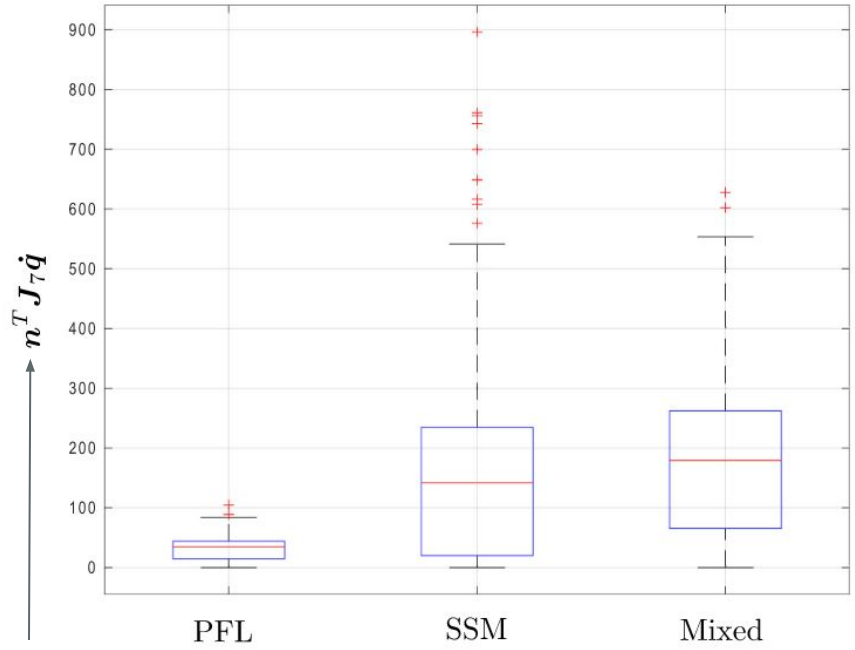

EE velocity

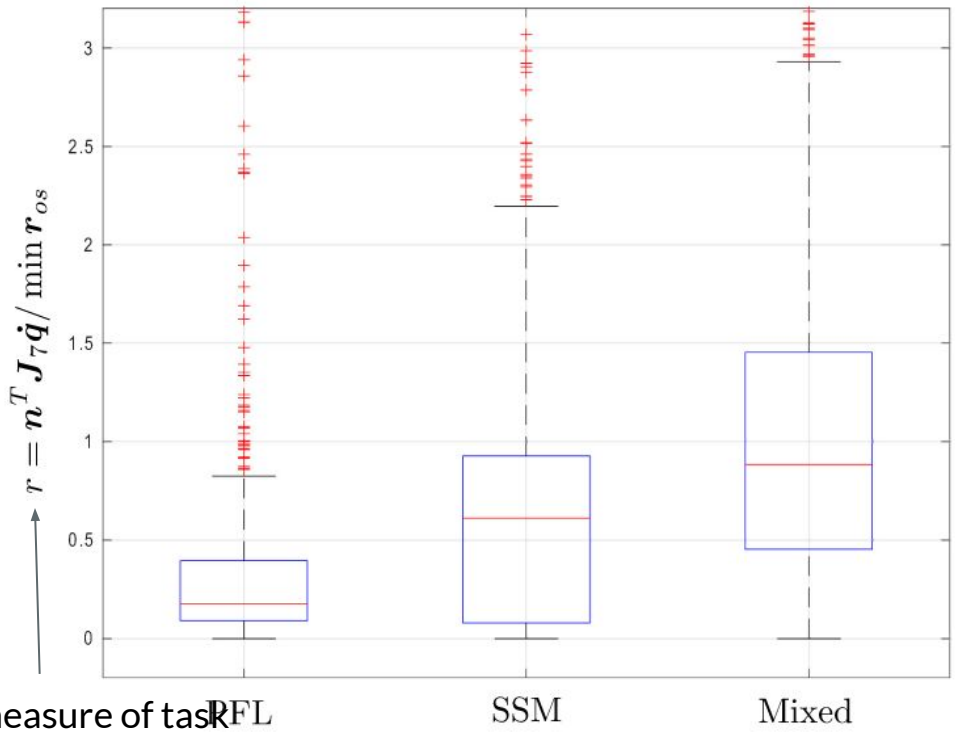

Specific measure of task independent velocity/distance ratio

Lucci, N., Lacevic, B., Zanchettin, A. M., & Rocco, P. (2020). Combining speed and separation monitoring with power and force limiting for safe collaborative robotics applications. *IEEE Robotics and Automation Letters*, *5*(4), 6121-6128.

Back to SSM & PFL together II - results

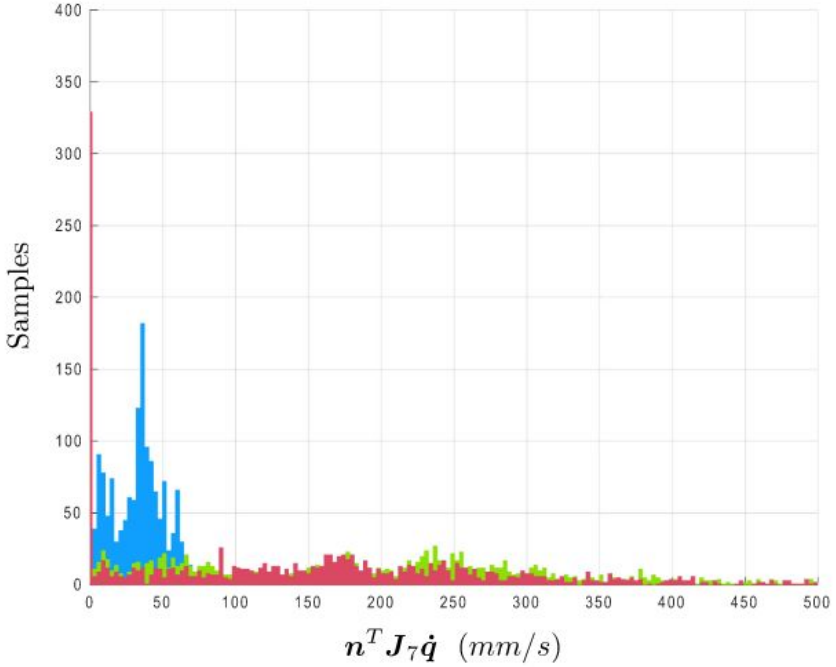

EE velocity

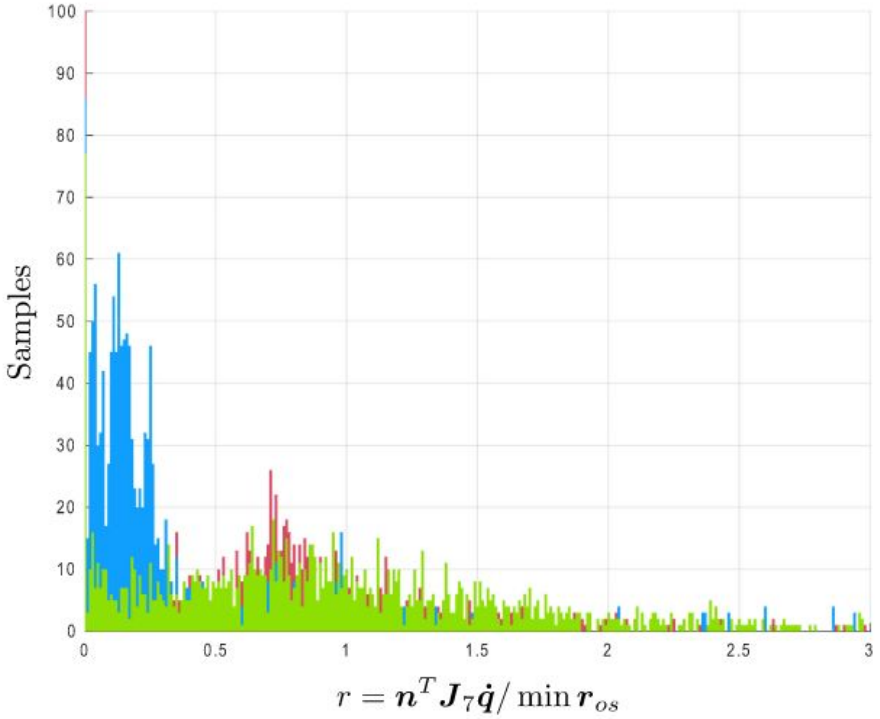

Specific measure of task independent velocity/distance ratio

Lucci, N., Lacevic, B., Zanchettin, A. M., & Rocco, P. (2020). Combining speed and separation monitoring with power and force limiting for safe collaborative robotics applications. *IEEE Robotics and Automation Letters*, *5*(4), 6121-6128.